CrossMark

Early Exposure to a High-Fat Diet Impacts on Hippocampal Plasticity: Implication of Microglia-Derived Exosome-like Extracellular Vesicles

Angeles Vinuesa [1,2] · Melisa Bentivegna [1,2] · Gastón Calfa [3] · Fabia Filipello [4] · Carlos Pomilio [1,2] · María Marta Bonaventura [2] · Victoria Lux-Lantos [2] · María Eugenia Matzkin [2] · Amal Gregosa [1,2] · Jessica Presa [1,2] · Michela Matteoli [4] · Juan Beauquis [1,2] · Flavia Saravia [1,2]

Abstract

Adolescence is a transitional period from childhood to adulthood characterized by puberty and brain maturation involving behavioral changes and environmental vulnerability. Diet is one of the factors affecting brain health, potentially leading to long-lasting effects. Hence, we studied the impact of early exposure (P21-60) to a high-fat diet (HFD) on mouse hippocampus, analyzing inflammation, adult neurogenesis, dendritic spine plasticity, and spatial memory. Glycemia and seric pro-inflammatory IL1β were higher in HFD mice without differences on body weight. In the HFD hippocampus, neuroinflammation was evidenced by Iba1+ cells reactivity together with a higher expression of TNFα and IL1β while the neurogenic capability in the dentate gyrus was strongly reduced. We found a predominance of immature Dil-labeled dendritic spines from CA1 neurons along with diminished levels of the scaffold protein Shank2, suggesting a defective connectivity. Moreover, the HFD group exhibited spatial memory alterations. To elucidate whether microglia could be mediating HFD-associated neuronal changes, the lipotoxic context was emulated by incubating primary microglia with palmitate, a saturated fatty acid present in HFD. Palmitate induced a pro-inflammatory profile as shown by secreted cytokine levels. The isolated exosome fraction from palmitate-stimulated microglia induced an immature dendritic spine phenotype in primary GFP+ hippocampal neurons, in line with the in vivo findings. These results provide novel data concerning microglia to neuron communication and highlight that fat excess during a short and early period of life could negatively impact on cognition and synaptic plasticity in a neuroinflammatory context, where microglia-derived exosomes could be implicated.

Keywords Hippocampus · Dendritic spines · High-fat diet · Microglia · Exosomes · Adolescence

Introduction

Science is today focusing greatly on adolescence, as the growing number of publications addressing the matter shows. This is not surprising since, at this moment, adolescents represent the largest cohort in human history [1]. Adolescence is considered a critical developmental period in life, characterized by the transition from childhood to adulthood, with important changes in brain architecture, puberty, and sexual maturity as well as the appearance of particular behaviors regarding sociability, risk-taking, reward sensitivity, and novelty-seeking [2, 3]. Importantly, these events are conserved across mammalian species, validating the use of mice models in the approach to this vital period [4]. An increase in anxiety-like behavior and enhanced sensitivity to stressors are commonly found during the adolescent period [5]. For this reason, the quality of the environment as a whole emerges as decisive. In this sense, physical activity, nutrition, and social interaction, among other factors, exert a strong influence on courses of health and development into later life [6].

Focusing on the nutritional environment, the higher consumption of industrialized food with high-fat content,

✉ Flavia Saravia
fsaravia@qb.fcen.uba.ar

1. Neurobiology of Aging, Departamento de Química Biológica, Facultad de Ciencias Exactas y Naturales, Universidad de Buenos Aires, CABA, Argentina

2. Instituto de Biología y Medicina Experimental, CONICET, Buenos Aires, Argentina

3. IFEC-CONICET, Departamento de Farmacología, Facultad de Ciencias Químicas, Universidad Nacional de Córdoba, Córdoba, Argentina

4. Laboratory of Pharmacology and Brain Pathology, Humanitas Clinical and Research Center, Milan, Italy

combined with sedentary habits, is associated with the rapid increase in overweight and obesity during adolescence and young adulthood across the world [7]. Several groups, including ours, have demonstrated that obesity and exposure to a high-fat diet (HFD) are connected with chronic systemic inflammation and dyslipidemia in humans and also in rodent models. Insulin resistance, coupled with the inflammatory response, is associated to increased cognitive decline, impaired spatial learning, and signs of depression. These symptoms are related to dysfunction of limbic structures such as the amygdala and hippocampus, crucial targets in brain aging and neurodegenerative diseases such as Alzheimer's disease [8–11]. Previous studies from our laboratory showed that HFD consumption was associated with decreased neurogenic ability in the hippocampal dentate gyrus in adult mice, with both a diminished proliferation and differentiation of newborn neurons in the subgranular zone (SGZ). Besides systemic inflammation, central inflammatory parameters were present in mice exposed to HFD, evidenced by activation of microglia, the innate immune cells of the CNS [12].

The last decades provided important evidence about microglial function: microglial cells do not only drive the inflammatory response upon different stimuli, they also provide regular neurotrophic support, acting as a key player in connectivity modulation by the remodeling and fine-tuning of synapses [13]. There are different mechanisms by which glial cells and neurons communicate. Apart from the well-established cell-to-cell contact associated to phagocytosis and pruning for instance, and the paracrine action of soluble mediators, glial cells and neurons can communicate by means of extracellular vesicles (EVs), a relevant phenomenon that accounts for cell function regulation across long distances [14–17]. In the literature, different EV classifications and nomenclatures can be found. However, the greater consensus regarding EVs biogenesis and size comprise microvesicles (MVs) and exosomes as the main types. MVs are 100- to 1000-nm-sized vesicles released by evagination of the cell membrane [18–20] and exosomes are nano-scaled vesicles with a diameter between 30 and 100 nm originated within multivesicular bodies (MVB) and released by MVB fusion with the plasmatic membrane. EVs biogenesis and release regulation may involve the participation of different components of the endosomal sorting complex required for transport (ESCRT) machinery, and exosome release can also be mediated by sphingomyelinase activity [21–23]. Aminopeptidase CD13, TSG101, ALIX, and the lactate transporter MCT-1 are considered specific markers for exosomes [24]. Among the cargoes transferred via EVs from one cell to another contributing to pathophysiological processes, pro-peptides, cytosolic proteins but also mRNA and micro RNAs are distinguished [25]. The state of the donor cell and the extracellular stimuli will strongly determine the composition and biological activity of EVs [26, 27]. In the CNS, this mechanism has been reported in the modulation of diverse phenomena affecting neuronal activity and communication with glial cells both in physiological conditions, as well as in the context of inflammation and the propagation of damage associated to neurodegenerative pathologies such as Alzheimer's disease and Parkinson's disease [28–32]. In a physiological scenario, microglia-derived EVs are shown to regulate synaptic transmission by different mechanisms such as sphingolipid metabolism enhancement in excitatory synapses and pre-synaptic transmission inhibition in GABAergic neurons when carrying components of the endocannabinoid system, among others [32]. Under brain inflammatory conditions, however, microglia is reported to respond by releasing different types of EVs. For instance, upon LPS activation, BV2 microglial cells are able to release EVs containing the pro-inflammatory cytokines TNFα and IL-6 [33]. Interestingly, microglial MVs can be detected in the cerebrospinal fluid of multiple sclerosis patients, [34] and they are able to propagate cytokine-mediated inflammatory responses across distant brain regions, being IL1β and GAPDH the main cargoes in ATP-induced microglial EVs release in culture [29, 35, 36]. Depending on the stimulus, EVs can potentially change their cargo and differentially influence synapses, being extracellular ATP a major stimulant for MV shedding in this cell type. Also, the analysis of exosomes from microglial culture exposed to injured brain extract revealed higher levels of miR-124-3p, apparently associated with a protective effect by inhibiting neuronal inflammation and promoting neurite outgrowth, being involved in neuroprotection and reduction of neuroinflammed status [37].

Given the relevance of microglia-neuron communication involved in several hippocampal plasticity-related processes, this work intends to get in-depth knowledge regarding this connection within a lipotoxic context associated to metabolic disorders. To our knowledge, information about the modulation of dendritic structural plasticity via microglial EVs in a hyperlipidic context is scarce or null. To address that, we performed a combined in vivo/in vitro approach. Mice exposed to a high-fat diet from weaning (P21) and up to the age of 2 months (P60) showed a more immature dendritic spine pattern in CA1 DiI-labeled neurons, in association to impaired spatial memory, decreased neurogenic ability, and marked inflammation in the hippocampus. In parallel, exosomes derived from primary microglia culture exposed to palmitate, the most representative saturated fatty acid in western diets, induced a clear preponderance of thin-type spines on primary hippocampal neurons, in remarkable similarity with the in vivo results. Therefore, from the results presented in this study, it can be suggested that metabolic-triggered neuroinflammation could contribute to modify neuronal connectivity in the hippocampus, with impact on cognitive behavior, where microglia-derived extracellular vesicles might represent possible glia-to-neuron damage mediators.

Taking into account the period in which these events were studied in vivo, corresponding to human adolescence, the effects could be determining for adult life.

Materials and Methods

Animals and Diets

C57BL/6J male mice (Jackson Laboratories, Bar Harbor, ME) were maintained in our animal facility (Institute of Biology and Experimental Medicine, UBA–CONICET; NIH Assurance Certificate # A5072–01) and were housed under controlled conditions of temperature (22 °C) and humidity (50%) with 12 h/12 h light/dark cycles (lights on at 7:00 am). All animal experiments followed the NIH Guide for the Care and Use of Laboratory Animals and were approved by the Ethical Committee of the Institute of Biology and Experimental Medicine. All efforts were done to reduce the number of mice used in the study as well as to minimize animal suffering and discomfort.

Three-week-old male mice (P21) were exposed to either the control or a high-fat diet during 6 weeks, as the experimental scheme shows (Fig. 1). We chose this particular time window of exposure since it thoroughly comprises the adolescent period when comparing this life stage to humans' relative age [38]. Both control diet (CD) and high-fat diet (HFD) were provided by Gepsa Feeds (Grupo Pilar, Pilar, Buenos Aires, Argentina). CD pellets provided 2.5 Kcal/g energy, whereas HFD pellets provided 3.9 kcal/g energy. CD pellets were composed by carbohydrate 28.8%, proteins 25.5%, fat 3.6%, fibers 27.4%, minerals 8.1%, and humidity 6.7%, while HFD pellets provided carbohydrate 22.5%, proteins 22.8%, fat 21.1%, fibers 23.0%, minerals 5.6%, and humidity 5.0%, as it was previously reported by our group [12] and Valdivia et al. using this diet [39].

During the last 2 weeks of exposure to the diet, the behavioral tests were performed as further described and euthanasia of the mice took place 3–5 days after the last behavioral task. At the end point, CD and HFD mice were weighed, 6-h fasted starting 1 h after the light period began, anesthetized with ketamine (80 mg/kg BW, i.p.;

Holliday-Scott, Argentina) and xylazine (10 mg/kg BW, i.p.; Bayer, Argentina), and then decapitated.

Tissue Processing

Pancreas was rapidly extracted, frozen in dry ice, and stored at − 80 °C until use for determination of insulin content.

Brains were removed from the skull, the left hemisphere dissected, and the hippocampus frozen in dry ice and stored at − 80 °C until use. A subgroup was processed for RT-qPCR and another for immunoblotting. Hippocampi that were used for Western blot were homogenized in supplemented RIPA buffer and those used for RT-qPCR were processed with trizol reagent as further detailed.

The right hemisphere was fixed overnight in the 4% para-formaldehyde (PFA) solution at 4 °C and then cut coronally at 60 μm in a vibrating microtome (Pelco easiSlicer, Ted Pella, USA). Sections were stored in a cryoprotectant solution (25% glycerol, 25% ethylene glycol, 50% phosphate buffer 0.1 M, pH 7.4) at − 20 °C until use. All immunohistochemical techniques were performed on free-floating sections. For cell number and morphometric analyses, six brain sections per mouse were evaluated. Ventral and dorsal hippocampi were considered, unless specified otherwise.

Pancreatic Insulin Content

As it was described in a previous report of our group [12] and others [40], CD and HFD pancreases were weighed and insulin was extracted from homogenates with acid-ethanol. Briefly, tissues were homogenized in 40 volumes of acid-ethanol (75% ethanol, 20% water, 5% acetic acid) and extracted overnight at 4 °C. Homogenates were centrifuged (10 min, 2000g, 4 °C) and the supernatants neutralized with 1 volume of 0.85 M Tris buffer. After a second incubation (60 min, − 20 °C) and centrifugation (30 min, 3000g, 4 °C), the supernatants were stored at − 70 °C until they were used. Pancreatic insulin was measured by radioimmunoassay (RIA) using human insulin for iodination and standard, provided by Laboratorios Beta, and anti-bovine insulin antibody (Sigma, St. Louis, MO). All samples were evaluated in the same RIA. The
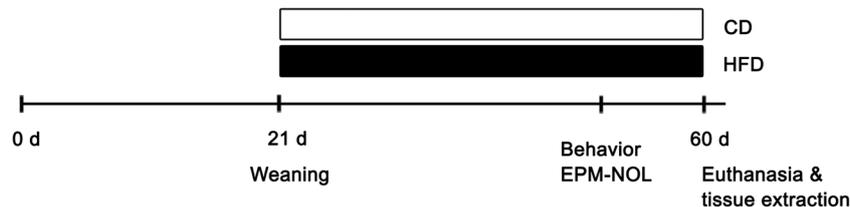
Fig. 1 Experimental scheme. C57BL/6J male mice were exposed to control (CD) or high-fat diets (HFD) since weaning (P21) until the onset of adulthood (P60). Elevated plus maze (EPM) and novel object location recognition test (NOL) were performed in the last 2 weeks of exposure. At the end point, CD and HFD mice were euthanized and the pertinent tissues were dissected for histological and biochemical analyses as detailed in the "Materials and Methods" section

minimum detectable concentration was 2 ng, and the intra-assay coefficient of variation was 6.8%. Pancreases from five to seven mice per group were used for insulin content determination.

Immunohistochemistry

Proliferation in the subgranular zone of the hippocampal dentate gyrus (DG) was studied by Ki67 immunolabeling. Doublecortin immunohistochemistry allowed the assessment of newborn neurons in the DG, and Iba1 immunohistochemistry was performed to assess morphometric parameters of microglia activation.

After blocking of nonspecific antigenic sites, sections were incubated overnight at 4 °C with the following primary antibodies: rabbit polyclonal anti-Iba1 (1:1500, Wako Pure Chemical Industries, Osaka, Japan), goat polyclonal anti-DCX (1:400, SC-8066, Santa Cruz Biotechnology, USA), or rabbit polyclonal anti Ki67 (1:2000 Novocastra/Leica, Germany).

We used biotinylated secondary antibodies (1:1000 Vector Laboratories USA) followed by processing with ABC kit (Vector Laboratories) and development with 2 mM diaminobenzidine (Sigma, USA) and 0.5 mM H_2O_2 in 0.1 M Tris buffer. Sections were placed on gelatin-coated slides, airdried overnight, dehydrated in graded solutions of ethanol, cleared in xylene, and mounted with Canada balsam.

For all immunostaining analyses, at least four brains per experimental group were used.

Ki67 Positive Cells in the SGZ

Ki67 immunostaining allowed the assessment of proliferation ability in the SGZ of the hippocampal dentate gyrus. Quantification of the number of Ki67+ cells was done under a ×40 objective in a Nikon E200 microscope. Every eighth 60-μm coronal brain section throughout the entire rostrocaudal extension of the DG was analyzed in each mouse. Cells were counted in both upper and lower blades of the SGZ and results were expressed as total Ki67+ cells per hemi-DG, taking into account whole or discriminating dorsal and ventral hippocampus.

DCX Positive Neurons and Differentiation in the SGZ

Doublecortin (DCX) immunohistochemistry was used to study adult neurogenesis. Quantification of the number of DCX+ cells was performed under a× 40 objective in a Nikon E200 microscope as it was previously reported by our group [12, 41]. Every eighth 60-μm coronal brain section throughout the entire rostro-caudal extension of the DG was analyzed in each mouse. Cells were counted in the SGZ and in the granular cell layer (GCL). Both upper and lower blades of

the GCL and SGZ were considered for cell counting and two different subpopulations of DCX+ cells were distinguished according to previously described criteria. A-D cells were defined as less mature DCX cells, with no apparent processes or short ones without exceeding the GCL, and E-F DCX+ cells were considered more mature neurons, with a primary dendrite and developed dendritic tree across the GCL and reaching the molecular layer of DG [42]. Results were expressed as total, A-D or E-F DCX+ cells per hemi-DG.

Microglial Density

Microglial density was estimated as it was already reported [43] using a randomly placed 6×10^5 μm³ counting probe on the hippocampal hilus. A minimum of 100 cells per animal were counted.

Microglial Soma Size

Soma size was evaluated as an indirect measure of microglial activation. Microphotographs from randomly chosen individual cells in the hippocampus hilus were obtained, the soma was delineated, and its surface quantified using the ImageJ software. At least 30 cells were measured in each animal.

Spine Analysis in DiI-Stained Brain Slices

Four HFD and four CD mice were deeply anesthetized with ketamine (80 mg/kg BW, i.p.; Holliday-Scott, Argentina) and xylazine (10 mg/kg BW, i.p.; Bayer, Argentina) and then transcardially perfused with 20 mL of 0.9% saline solution, followed by 20 mL of 4% PFA in 0.1 M phosphate buffer, pH 7.4. Brains were removed from the skull and further post-fixed with the same fixative for 24 h at 4 °C. Afterwards, brains were coronally cut at 150 μm with a vibrating microtome in order to obtain slices containing mainly the dorsal hippocampus. CA1 neurons from the dorsal hippocampus were stained with a saturated solution of DiI (1,1′dioctadecyl-3,3,3′,3′-tetramethyl indocarbocyanine perchlorate) (Invitrogen, USA) in fish oil [44]. As it was previously published [45], the dye was microinjected using a glass patch clamp pippette attached to a micromanipulator and introduced in the cells by means of positive pressure. Stained sections were incubated in the dark at RT for 24 h, post-fixed in 4% PFA for 2 h at RT, adequately washed with PBS, and mounted in a Vectashield medium (Vector Laboratories; Burlingame, CA). To perform dendritic spine analysis, z-stack images with 0.1 μm step size were acquired with a confocal microscope Olympus FV-300 (Centro de Microscopía Óptica y Confocal de Avanzada, Universidad Nacional de Córdoba, Argentina), ×60 oil immersion objective (NA 1.42). Z-stacks were deconvolved using the Huygens Professional software (Scientific Volume Imaging, Leica, Netherlands), with the advanced maximum

likelihood algorithm, set with 15 iterations. Dendritic spine density and morphology were assessed in dendritic segments of secondary or tertiary apical dendrites from CA1 neurons, using the ImageJ software (NIH, USA), and spine category classification was done automatically using theoretical parameters of spine length, head and neck diameters, using previously reported criteria (Table 1). Briefly, spine types were classified considering the length (dimension from the base at the dendrite to the tip of its head, L), the diameter of the neck (measured as the maximum neck diameter, dn), and the diameter of the head (measured as the maximum head diameter, dh). Thus, individual spines were included in each category based on the specific ratios L/dn and dh/dn [46]: type I or "stubby"-shaped dendritic spines, type II or "mushroom"-shaped dendritic spines, and type III or "thin"-shaped dendritic spines. Generally, stubby spines present an L similar to the dn and the dh, and in general the magnitude is < 1 μm. Mushroom spines present a dh much larger than the dn in which the L is typically < 1 μm. Thin spines present an L longer than 1 μm that is much greater than the dn [46–48]. Spine density was normalized to 10 μm of dendritic segment, analyzing a total of at least 1200 μm per group.

Immunoblotting

Frozen hippocampi and BV2 cell lysates were homogenized by sonication in supplemented RIPA buffer. Protein quantification of the homogenates was obtained by the Bradford standardized method [49]. After lysis with loading buffer 5×, samples were loaded on 10 or 7.5% acrylamide gels, separated by SDS-PAGE, and then transferred to nitrocellulose membranes. Membranes were blocked with 5% nonfat milk in TBS containing 0.5% Tween-20 (TTBS). To assess synaptic marker levels, membranes were incubated overnight at 4 °C with mouse monoclonal PSD-95 (1/500, 7E3, SC32290, Santa Cruz, USA), rabbit polyclonal Shank 2 (1/500, catalog number 162202, Synaptic Systems, Germany) and mouse monoclonal β-Actin (1/500, C4, SC-47778, Santa Cruz, USA) antibodies. For determination of exosomal markers in BV2 cell lysates and the derived exosome fraction,

membranes were incubated with mouse monoclonal ALIX (1/250, 3A9, SC-53538, Santa Cruz, USA) and mouse monoclonal TSG101 (1/250, C2, SC-7964, Santa Cruz, USA). After initial probing with primary antibodies, membranes were washed in 0.5% TBST and TBS solutions, incubated for 1 h with 1:1000 dilutions of species-appropriate, HRP-conjugated secondary antibodies (Bio-Rad, USA). After washing, immunoreactivity was visualized by reaction in ECL detection reagents (luminol and p-coumaric acid; Sigma-Aldrich Co., St. Louis, MO, USA) for 3 min, followed by immediate exposure of the blot using Amersham Imager 600 RGB (GE Healthcare, USA). Bands at the relevant molecular weights were quantified using the ImageJ plug-in for gel analysis. Ratios of synaptic proteins to actin levels were used to compare CD and HFD experimental groups.

Real-Time PCR of TNFα and IL1β

Hippocampi were homogenized by sonication in Trizol reagent (Life Technologies-Invitrogen, CA, USA) and total RNA was extracted as recommended by the manufacturer. The concentration and purity of total extracted RNA was determined by measuring the optical density of the samples at 260 and 280 nm in a Nanodrop 2000 (Thermo Scientific USA). cDNA templates for PCR amplification were synthesized from 1 μg of total RNA using a MMLV High Performance Reverse Transcriptase enzyme (Epicenter, USA) for 60 min at 37 °C in the presence of random hexamer primers. The sequences of primers for amplification of mouse TNFα, IL1β, and cyclophilin B are shown in Table 2. Cyclophilin B was used as reference gene or housekeeping, based on the regularity of its expression between experimental groups. PCR protocols were optimized for each gene, being 10 min at 95º C and 40 cycles at 95 °C for 15 s followed by 60 °C for 1 min for cyclophilin B; 10 min at 95º C and 40 cycles at 95 °C for 20 s followed by 58 °C for 30 s and at a 72 °C for 1 min for TNFα; and 10 min at 95º C and 40 cycles at 95 °C for 20 s followed by 60 °C for 30 s and at a 72 °C for 1 min for IL1β.

Samples were measured with a Bio-Rad CFX (Hercules, CA, USA) detection system in a reaction mixture with a final volume of 15 μl, containing 10 μl SYBR® Select Master Mix (Thermo Fisher). Eight hippocampi were used per group and every reaction was done in duplicate. Relative expression was calculated by Pfaffl's method [50] as shown by the equation below and expressed as fold increase in relation to the control group (CD).

$$\text{Relative expression} = \frac{\left(E_{\text{target}}\right)^{\Delta Ct_{\text{target}}}}{\left(E_{\text{reference}}\right)^{\Delta Ct_{\text{reference}}}},$$

where E is primers' efficiency for each target and reference gene, and ΔCt is obtained as the difference between the

Table 1 Ratio criteria for spine morphology classification[46]

L/dn	dh/dn		
	(0, 1.3)	(1.3, 3)	(3, ∞)
(0, 2/3)	Stubby	Mushroom	Mushroom
(2/3, 2)	Stubby	Stubby	Stubby
(2, 3)	Stubby	Mushroom	Mushroom
(3, 5)	Thin	Mushroom	Mushroom
(5, ∞)	Thin	Thin	Thin

Table 2 Sequence of primers used in RT-qPCR

Gene	Forward primer sequence 5′- 3′	Reverse primer sequence 5′- 3′
TNFα	GAAAAGCAAGCAGCCAACCA	CGGATCATGCTTTCTGTGCTC
IL1β	AACCTGCTGGTGTGTGACG	CAGCACGAGGCTTTTTTGTT
Cyclophilin B	AAGCATACAGGTCCTGGCATCT	CATTCAGTCTTGGCAGTGCAG

control group average Ct and the mean of every sample for each corresponding gene. Amplification specificity was verified by dissociation curves' analysis. Primers were used at a concentration of 0.3 μM and cDNA in a 1:5 dilution.

Behavioral Procedures

General Considerations

Animals were tested during the light period, between 8:00 and 14:00 h. The order of testing was first the elevated plus maze (EPM) and then the novel object location recognition test (NOL) within 1 week separation. At least 10 CD and 10 HFD animals were tested.

Elevated Plus Maze

The elevated plus maze was performed as previously reported, to assess anxiety [12]. It consisted of four 30-cm arms, two open and two closed, elevated 50 cm from the ground. After a 15-min adaptation to the testing room, mice are allowed to explore the maze during 10 min, recorded by a video camera. Upon video analysis, exploration time was quantified.

Novel Object Location Recognition Test

Novel object location recognition test was performed in order to analyze the hippocampus-dependent spatial memory and was carried out as previously published [12, 41]. Briefly, mice were habituated to the test arena ($30 \times 30 \times 30$ cm^3 black box) in the behavior room for 5 days before the test. The first day consisted of a 5-min group exploration session in the box, and an individual 10-min exploration session on the following four consecutive days. The day of the test, mice were subjected to two object exploration 10-min trials within the known boxes, T1 and T2, separated by a 60-min inter-trial interval (ITI). Objects were identical and one of them was relocated in T2. Object preference was analyzed in the acquisition phase (T1), measured as the percent difference in the exploration of each object, relative to total T1 exploration time (one-sample t test against theoretical mean of 0). Locomotor activity, measured as total distance and average speed, was assessed with the Any-maze video tracking system

(Stoelting Co, USA). Novel location exploration was evaluated in comparison to random exploration (one-sample t test against 50% chance level) and with a discrimination index, as the percent difference in T2 exploration of novel and known objects, relative to total T2 exploration time (two-sample t test comparing experimental groups).

Cell Cultures

Both microglial and neuron primary cultures were obtained as previously reported by Matteoli's group [35, 51].

Primary Microglia

Microglial cells were mechanically detached from mixed glial cultures. Briefly, P1-3 C57BL/6J pups were decapitated, brains were removed from the skull, and the cortices and hippocampi were dissected. After exhaustive removal of meninges and a first step of mechanical tissue disaggregation, cortices were subjected to two rounds of enzymatic dissociation with 0.1% DNase (Sigma, USA), 0.025% trypsin (Sigma, USA) in Hank's Balanced Salt Solution (HBSS) at 37° C for 15 min in agitation. Enzymatic activity was neutralized with Minimum Essential Medium (MEM) with Earle salts (Thermo Fisher Scientific, USA) supplemented with 20% fetal bovine serum (FBS). The cell suspension was filtered through a 70-μm pore cell strainer (Corning, USA) and then centrifuged at 800g for 10 min. The cell pellet was then resuspended in complete cell culture medium (MEM, 20% FBS, 0.6% glucose, 100 units/mL penicillin, and 100 mg/mL streptomycin), seeded in T75 flasks and maintained in a humid atmosphere at 37 °C, 5% CO$_2$, and 95% air. After 10–14 days in culture when the monolayer of astrocytes was formed, microglial cells were obtained by orbital shaking at 240 rpm for 45 min. The resultant supernatants were centrifuged at 800g, cells were resuspended, counted and seeded in previously poly-L-ornithine-coated plates at a density of 700 cells/mm^2, and maintained in the mentioned glial medium and incubation conditions.

Primary Hippocampal Neurons

Primary hippocampal neurons were obtained from E18 C57BL/6J mouse brains. Briefly, as previously detailed for glia cultures, brains were obtained and meninges carefully removed. Hippocampi were dissected and chemically dissociated with 0.025% trypsin in HBSS, during 15 min at 37 °C and further mechanical disaggregation. The reaction was neutralized with the Neurobasal medium (Thermo Fisher Scientific, USA) supplemented with 10% FBS and cells were seeded in poly-L-lysine-coated coverslips at a density of 400 cells/mm^2. Cultures were maintained in the Neurobasal medium supplemented with 2% B27 (Thermo Fisher Scientific, USA), 2 mM glutamine, 12.5 µM glutamate, 100 units/mL penicillin, and 100 mg/mL streptomycin, in a humid atmosphere at 37 °C, 5% CO_2, and 95% air.

Palmitate Preparation

Palmitic acid (PA) (Sigma, USA) was dissolved at a concentration of 150 mM in 50% ethanol/water solution at 60° C. Afterwards, complexes of palmitate and 10% free fatty acid (ffaa) BSA *W/V* in water (Sigma, USA) were obtained in a 5:1 ratio by stirring the solution for 1 h at 37 °C, generating a 7.5-mM palmitate-10% ffaa BSA stock solution that was sterile filtered and kept at − 20° C until use [52]. Palmitate working solutions were prepared fresh for each experiment by diluting the stock in 2% FBS glial medium into 500 and 125 µM palmitate concentrations.

Viability Assay by DAPI/PI Staining

Palmitate-exposed microglial viability was assessed by DAPI (2 µg/mL) /PI (1 µg/mL) staining. Cells were seeded in a 24-well plate and stimulated with vehicle, 125 or 500 µM PA solutions for 24 h and incubated with DAPI/PI within the last 15 min of exposure. Using an inverted Olympus IX53 fluorescence microscopy (Humanitas Research Hospital, Milan, Italy), images were taken from at least three different fields from two independent experiments in order to analyze the proportion of dead, PI positive cells, upon palmitate exposure. The ImageJ (NIH, USA) software was used to analyze DAPI/PI nuclei.

Cytokine Levels

TNFα, IL1β, and IL4 levels were measured by ELISA in the supernatants of palmitate-exposed microglia. The following PeproTech ELISA kits were used: Standard ABTS ELISA Developmental kit (catalog number 900-K54) for mouse TNFα, mouse IL1β ELISA Developmental kit (catalog number 900-K47), and mouse IL4 ELISA Developmental kit (catalog number 900-K49), following the manufacturer's instructions. Determinations were performed in triplicate from at least three independent experiments. After absorbance values were obtained from a plate spectrophotometer, cytokine levels were determined using the corresponding standard curve for each cytokine and values were normalized to the control, thus setting the control condition as 1. One- sample Student t test against a theoretical mean of 1 was performed for statistical analysis.

Extracellular Vesicles' Isolation

Extracellular vesicles (EVs) were obtained from the conditioned media of 24 h-vehicle or palmitate-exposed microglia. For this purpose, 2×10^6 microglial cells were seeded in 60-mm petri dishes coated with poly-L-ornithine, and EVs were isolated from 3 mL of glial medium supplemented with 2% FBS that was previously ultracentrifuged for 18 h for thorough serum extracellular vesicles' depletion [53]. EVs isolation was done by differential centrifugation and every centrifugation and ultracentrifugation step was performed at 4° C. As it is shown in the scheme (Fig. 7a), the first centrifugation step at 800g for 5 min allowed the removal of cell debris (P1) and the resultant supernatant was centrifuged at 4000g for 20 min to obtain organelles and apoptotic bodies (P2). In order to obtain microvesicles of 100–1000 nm diameter (MVs or P3), the supernatant was centrifuged at 15,000g for 60 min. Finally, the fraction corresponding to exosome-like vesicles of 30–100 nm diameters (P4) was purified by ultracentrifugation (Beckman ultracentrifuge, SWTi55 rotor) at 110,000g for 90 min. Pellets of vesicles that were further used for functional or biochemical assays were washed in PBS following the same centrifugation conditions upon which they were obtained. EVs were resuspended either in PBS for functional assays (hippocampal neuron stimulation) and electron microscopy, or lysis buffer for protein determinations with the Micro BCA Protein Assay Kit (Thermo Fisher Scientific, catalog number 23235).

For Western blot determination of EV markers, protein extraction was performed by using the same isolation protocol but from the BV2 microglial cell line, in order to optimize protein yield. BV2 cell line was maintained in RPMI 1640 (Gibco, USA) 10% FBS, 100 units/mL penicillin and 100 mg/mL streptomycin, in a 5% CO_2 incubator. For this experiment, 1×10^6 cells were seeded in 60-mm petri dishes in RPMI with 2% FBS that was previously ultracentrifuged for 18 h. EVs isolation was performed 48 h after seeding, using 3 mL of collected conditioned media from 24-h vehicle or PA-exposed cells.

Electron Microscopy

For morphologic assessment of purified EVs, vesicles were visualized by transmission electron microscopy (TEM) in

LANAIS-MIE (Laboratorio Nacional de Investigación y Servicios de Microscopía Electrónica, UBA-CONICET, Argentina). Ten microliters of each suspension were deposited over a grid with a hydrophilic LRW membrane. Afterwards, 2% uranyl acetate staining was performed for 3 min, followed by bi-distilled water washes and room temperature drying until seen under transmission electron microscopy (Zeiss EM 109T with digital camera Gatan ES1000W, LANAIS-MIE IBCN CONICET).

Hippocampal Neuron Transfection and Spine Analysis

In order to perform dendritic spine analysis, 12 DIV hippocampal neurons were transfected with pEGFP-C1 plasmid using Lipofectamine 2000 (Thermo Fisher Scientific, USA) in a Neurobasal medium without serum. Neurons were incubated with the DNA-Lipofectamine complexes for 30 min at 37 °C and then were transferred to their original medium. After 48 h, neurons were exposed to the different fractions of EVs corresponding to palmitate- or vehicle-treated microglia for 24 h. Neurons were then fixed with 4% PFA for 10 min, washed in PBS. and mounted with PBS/glycerol medium. Neurons were analyzed using a FV1000 Olympus confocal microscope (Humanitas Research Hospital imaging facility). Z-stacks from GFP+ dendritic trees were obtained using a ×60 oil immersion objective (NA 1.42) with a 0.4 step size in z-axis. Using the ImageJ software, reconstruction of z-stacks was performed in order to analyze dendritic spine densities and morphology, normalized to 10 μm of secondary/tertiary segment, as it was previously explained in the "Materials and Methods" section for DiI tissue staining. Segments from at least 15 neurons per group were analyzed, in two independent experiments and statistical analysis was performed by one-way ANOVA followed by Tukey post hoc comparisons.

Statistical Analysis

Data are expressed as mean ± SEM. Analysis were performed under blind condition to the experimental groups. Statistical analyses were performed using unpaired one-tailed Student's t test (for one sample or comparing two samples) and one-way ANOVA with Tukey post hoc multiple comparisons when required and were done using Prism 3.02 (GraphPad Software).

Sample size for the animal studies was calculated taking into consideration results from previous studies done in our laboratory [12, 43]. For a statistical significance level of 5% and an 80% statistical power using a one-tailed Student's t test, we are able to detect differences of at least 10% between groups composed by 5 mice each for RIA; 4 for immunohistochemistry, WB, and DiI; 8 for qPCR; and 10 for behavioral evaluation. Analyses were done using the sample size calculation tool on StatMate 2.0 (GraphPad Software Inc.).

Results

Early Exposure to a High-Fat Diet Impacts on Metabolic and Inflammatory Parameters with no Changes on Body Weight

As it was previously reported by our group, after a short exposure to HFD (45% Kcal from lipids), from 21 to 60 days of life, no variations on final body weight were registered, whereas glycemia was increased in the HFD group compared to the control group fed with the standard diet [12]. In the present work, we report that pancreatic insulin content measured by RIA (1.78 ± 0.14 ng/mg vs. 1.36 ± 0.05 ng/mg) was found significantly decreased after HFD exposure, $p < 0.05$ Students' t test. Regarding systemic inflammation, there was approximately a tenfold increase in plasmatic levels of IL-1β ($p < 0.05$) while TNFα did not change [12].

As for the inflammatory status in the hippocampus, cytokine expression levels were assessed as well as microglial morphometric parameters. Firstly, Iba1 immunolabeling on coronal brain slices containing hippocampus allowed microglial activation assessment (Fig. 2a–f). No changes were detected in cell density (Fig. 2c–d), while an enlarged Iba1+ soma size was found both in the hilus (Fig. 2e) of the dentate gyrus ($p < 0.01$) and in the stratum radiatum subregion of CA1 (Fig. 2f, $p < 0.05$), as a sign of reactivity. Moreover, the expression of pro-inflammatory cytokines TNFα and IL1β measured by RT-qPCR was found to be increased in hippocampus homogenates of the HFD group (Fig. 2g–h, $p < 0.05$).

Fat Consumption Promotes Alterations in Adult Neurogenesis and Hippocampal Connectivity

Concerning neuronal impact of early HFD consumption, adult neurogenesis was one of the studied phenomena. The effect of the hyperlipidic diet on the neurogenic ability in the hippocampal SGZ was assessed in relation to two important stages of the neurogenic process: proliferation and differentiation of newborn cells in the subgranular cell layer of the dentate gyrus. To that purpose, proliferation marker Ki67 (Fig. 3a–b) and marker of immature neurons DCX (Fig. 3f–g) were studied by immunohistochemistry. In our work, the HFD group exhibited alterations in both proliferation, assessed as the number of Ki67+ cells in dorsal and ventral hippocampus (Fig. 3c–e, $p < 0.01$), and in the number of DCX+ immature neurons (Fig. 3h, $p < 0.01$) in the SGZ, being lower in the experimental group when taking into account the entire hippocampus. No significant differences were found when discriminating dorsal or ventral hippocampus (Fig. 3i–j). Taken together, these results suggest a decreased ability to generate new neurons in the hippocampus of mice exposed to HFD, considering an age at which neurogenesis normally occurs at a particularly high rate [54]. As regards DCX+ neurons, the
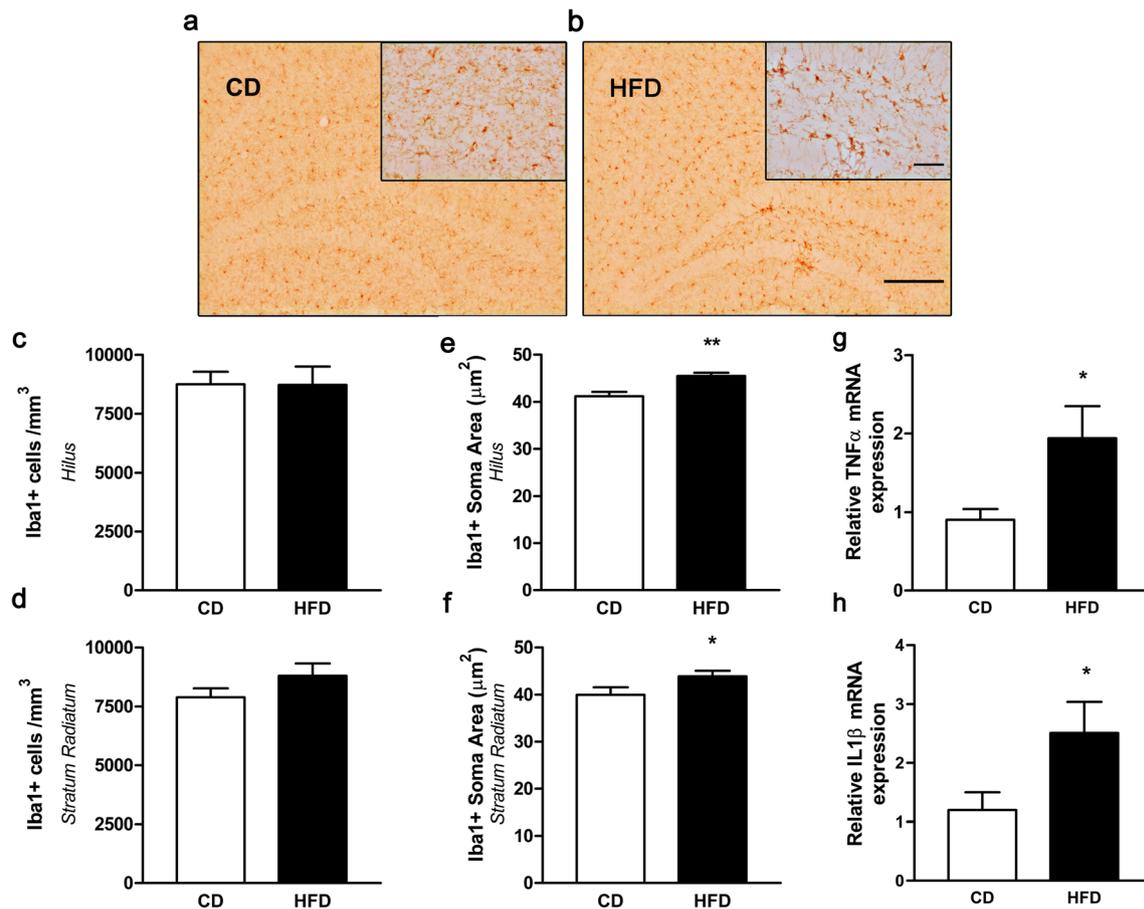
Fig. 2 HFD exposure induces inflammatory changes in the mouse hippocampus. **a**, **b** Representative images of Iba1 immunohistochemistry in coronal brain slices, and their corresponding insets of the hippocampal hilar region (scale bars = 100 and 50 μm, respectively). **c**, **d** Iba1+ cell density in the hilus (**c**) and stratum radiatum (**d**), expressed as number of cells per cubic millimeter. **e**, **f** Iba1+ cells' soma area in the hilus (**e**) and stratum radiatum (**f**).

$*p < 0.05$ and $** \; p < 0.01$ when compared to CD (Student's t test), $n =$ 4–5 CD and HFD mice. **g**, **h** Relative expression of TNFα (**g**) and IL1β (**h**) cytokines measured by RT-qPCR. Expression analysis was performed by Pfaffl's method and values were normalized to cyclophilin B as housekeeping gene and relative to the CD group. $*p < 0.05$ when compared to CD (Student's t test), $n = 8$ hippocampi per group

differentiation process was further analyzed by distinguishing A-D and E-F populations (as described in the corresponding "Materials and Methods" section) and we found a significant decrease particularly in A-D, the more immature ones (Fig. 3k, $p < 0.05$), not in E-F that presents greater development of dendritic trees (Fig. 3l).

With the aim to explore whether the high-fat diet could influence the synaptic compartment, morphological parameters of dendritic spines were evaluated after injection of DiI, a photostable lipophilic dye, for individual neuron staining (Fig. 4a). Fluorescent labeling of dendrites and spines followed by confocal microscopy allowed the imaging of dendritic spines with high resolution. After deconvolution of confocal z-stack images of dendritic segments (Fig. 4c–d), we were able to visualize individual spines in order to accurately determine each spine's length, head and neck diameter, allowing the morphological classification of spines (Fig. 4b): stubby (type I), mushroom (type II), or thin (type III), as described in the "Materials

and Methods" section. For interpretation purposes, it is important to mention that we enclose stubby spines in the "mature" category, together with mushroom spines, owing to a growing body of literature that consider both types to be more stable and to form stronger excitatory synapses [45, 47, 48, 55, 56], even if the majority of spines in this category are mushroom. Our results showed that, without changes in the total density of dendritic spines (Fig. 4e), there was a lower proportion of mature protrusions (types I + II, Fig. 4f, $p < 0.05$), mushroom spines in particular (type II, Fig. 4g, $p < 0.01$) in young mice consuming HFD compared with the standard diet, with a prevalence of immature thin dendritic spines (type III, Fig. 4h, $p < 0.01$). In order to further study this phenomenon, synaptic proteins associated to the postsynaptic density region (PSD) were analyzed by Western blot of CD and HFD hippocampal homogenates (Fig. 4i). Even if differences were not found in the levels of PSD-95 (Fig. 4k), a 50% decrease was detected for Shank 2 in HFD hippocampi (Fig. 4j, $p < 0.05$).
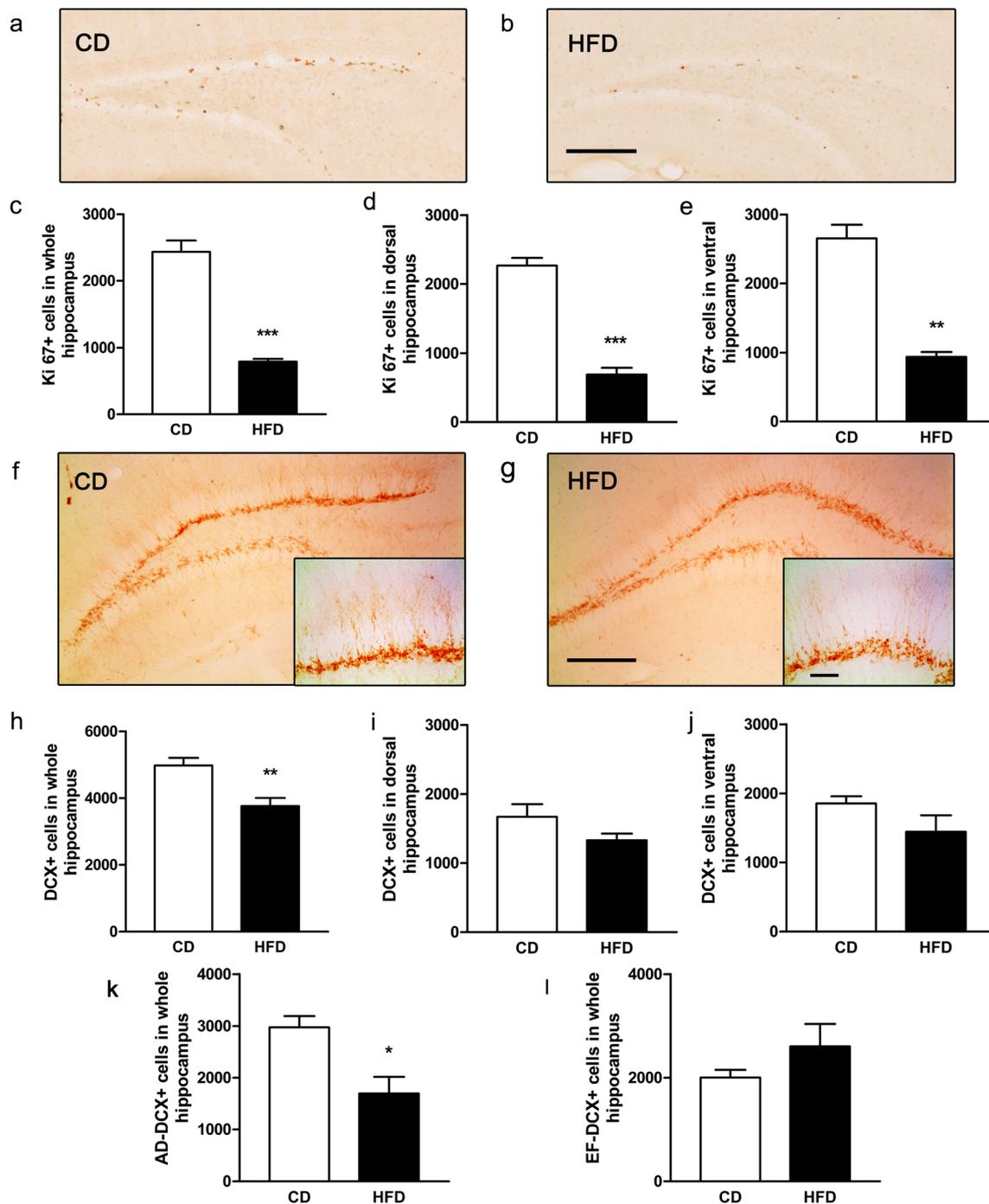
Fig. 3 Neurogenic ability is decreased in the dentate gyrus SGZ of HFD mice. **a**, **b** Representative images of Ki67 immunostaining in CD (**a**) and HFD (**b**) groups (scale bar = 200 μm). **c–e** Number of Ki67+ cells in the dentate gyrus SGZ, analyzing whole (**c**), dorsal (**d**), or ventral (**e**) hippocampus. **f**, **g** Photographs of DCX immunostaining and their corresponding SGZ insets, of CD (**f**) and HFD (**g**) groups (scale bars = 200 and 50 μm, respectively). **h–l** Number of total DCX+ cells in SGZ analyzing whole (**h**), dorsal (**i**), or ventral (**j**) hippocampus. A-D (**k**) or E-F (**l**) subpopulations of DCX+ cells in SGZ in the whole hippocampus. *$p < 0.05$, **$p < 0.01$, and ***$p < 0.001$ when compared to CD (Student's t test), $n = 4$–5 animals per group

High-Fat Diet Exposure Induces Spatial Memory Impairment in Young Mice

To address the potential effect of early fat consumption on hippocampus-dependent spatial memory, the novel object location recognition test was employed. As detailed in the corresponding "Materials and Methods" section, after adequate habituation, each mouse freely explored two identical objects during 10 min (T1), located as is illustrated in Fig. 5a. After this first training session, mice were returned to their housing cages. Sixty
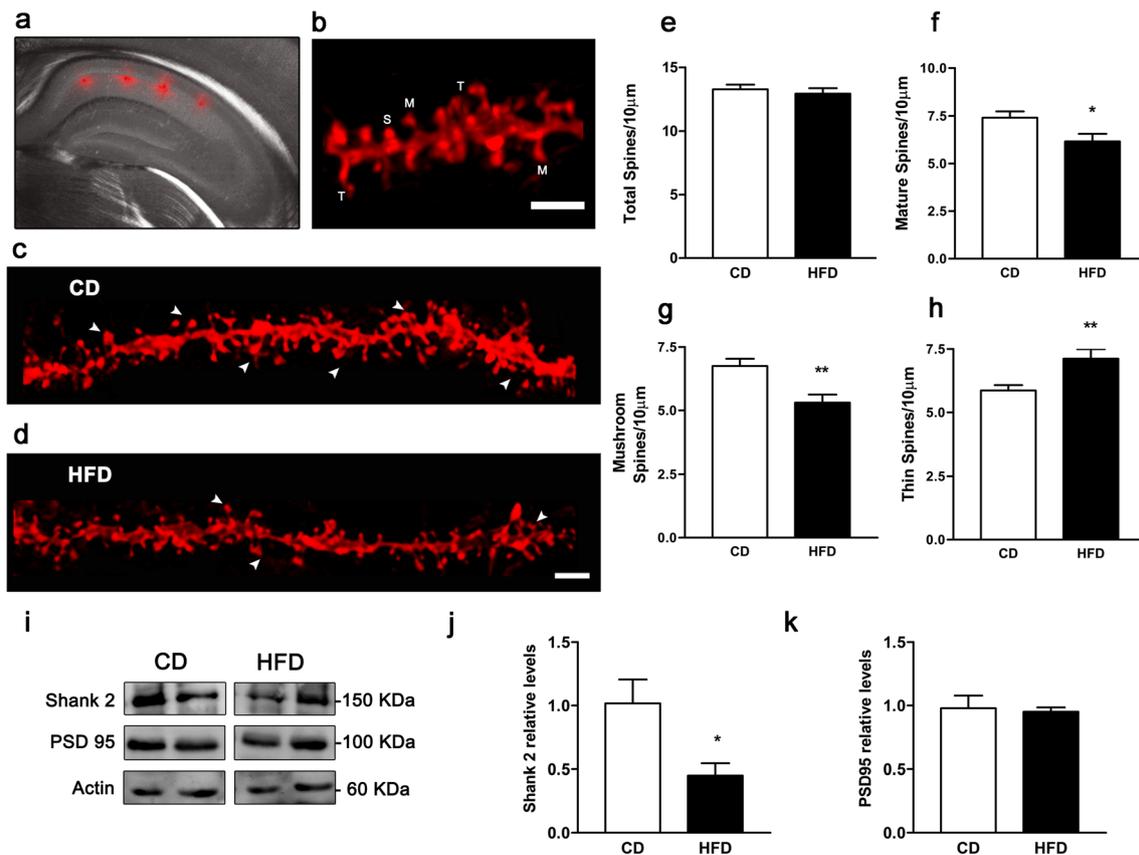
Fig. 4 HFD mice exhibit alterations in the morphology of dendritic spines of dorsal hippocampus CA1 neurons. **a** Representative photograph of a 150-μm coronal brain section showing injection sites of lipophylic Dil dye, seen as red fluorescence in CA1 pyramidal neurons, merged with the DIC microscopy image. **b** Reconstruction of the dendritic segment from deconvolved z-stacks obtained with confocal microscopy, showing examples of stubby (S), mushroom (M), and thin (T) dendritic spines (scale bar = 2 μm). **c, d** Representative 3D reconstructions of DiI-stained apical dendritic segments from CA1 neurons, from the CD (**c**) and HFD (**d**) groups, respectively. Arrows show mature, mushroom spines (scale bar = 2 μm). **e–h** Number of dendritic spines normalized to the 10-μm dendritic segment. Total dendritic spines (**e**), mature (stubby + mushroom) (**f**), mushroom (**g**), or thin (**h**) spines. $*p < 0.05$ and $**p < 0.01$ when compared to CD (Student's t test), $n = 4$ CD and HFD animals, analyzing at least 1200 μm dendritic length per group. **i–k** Representative Western blot bands showing the levels of Shank2, PSD-95, or actin in hippocampal homogenates from CD or HFD mice (**i**) and the corresponding densitometry analysis of Shank2 (**j**) or PSD-95 (**k**), relative to actin levels. $*p < 0.01$ when compared to CD (Student's t test), $n = 4$ CD and HFD hippocampi, results from three independent blots

minutes later, the second trial was registered on the same arena but with a different object spatial configuration (T2) (Fig. 5a). As expected, the control group showed a significant increase in time exploring the relocated object during T2, suggesting the recognition of this novel location (Fig. 5b, $p < 0.001$, one-sample Student's t test against 50%). Even if the HFD group was also able to recognize the novel location, as shown by the exploration percentage above randomness (Fig. 5b, $p < 0.05$), the discrimination index was significantly lower (Fig. 5c, $p < 0.01$). The discrimination index describes the difference between the proportion of time spent exploring an object placed in the novel location and the proportion of time visiting the object in the original location during T2, related to the total time spent in exploring both objects. It is important to mention that preference for no particular object was verified in T1 ($-0.70 \pm 4.40\%$ and $9.17 \pm 4.32\%$ preference index in the CD and HFD groups, respectively, one-sample t test against theoretical mean of 0,

$p > 0.05$) and locomotion impairment was discarded by distance and speed analyses measured with the Any-maze video tracking system (16.43 ± 1.84 m vs. 15.18 ± 1.24 m CD and HFD total distance; 0.03 ± 0.0031 m/s vs. 0.03 ± 0.0021 m/s CD and HFD exploration speed, two-sample t test, $p > 0.05$ between experimental groups). Hence, regarding this specific test, HFD mice exhibited impairment in short-term spatial memory. In relation to anxiety-like behavior, at least assessed by the elevated plus maze exploration test (Fig. 5d), no differences were found between experimental groups in the exploration of open arms (Fig. 5e).

Saturated Fatty Acid Palmitate Induces a Pro-inflammatory Profile in Cultured Microglia

The in vivo experiments showed that an early exposure to a HFD is associated to a pro-inflammatory response involving microglial cells in the hippocampus, together with poor
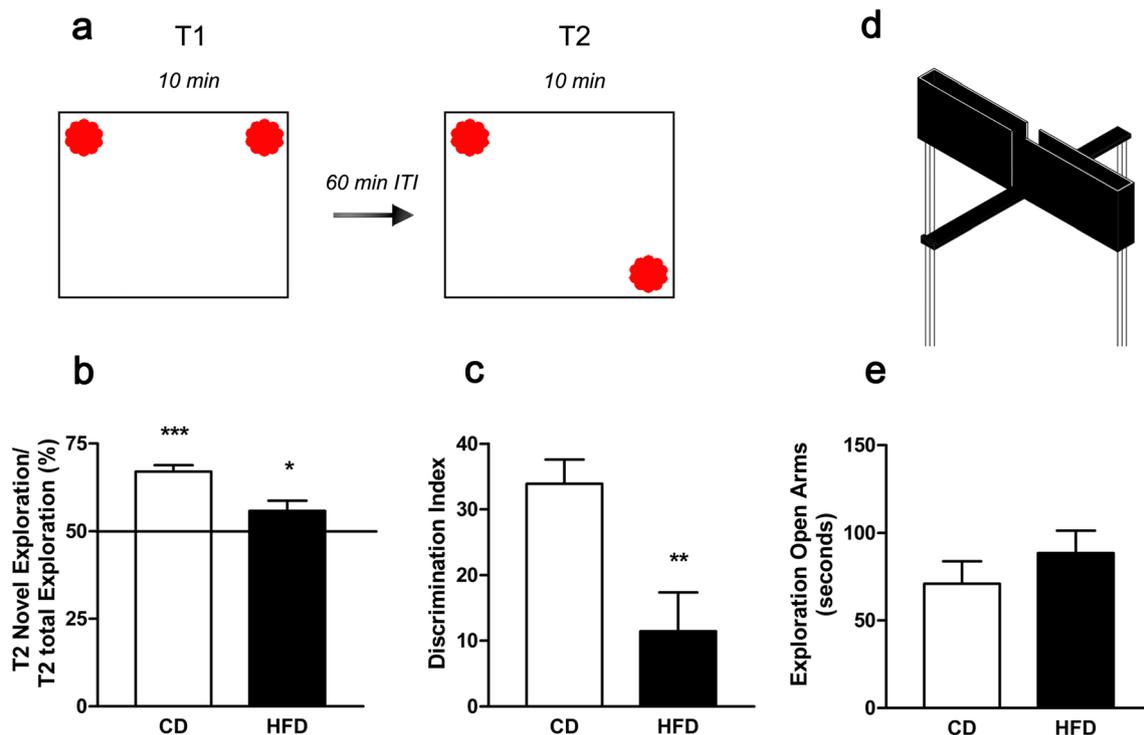
Fig. 5 Behavioral parameters. Early exposure to HFD promotes deficits in spatial memory. **a** Novel object location recognition test scheme showing objects' spatial configuration in T1 and T2 sessions and intertrial interval (ITI). **b** Quantification of the exploration time of the re-localized object, expressed as percentage of total exploration in T2. $*p < 0.05$ and $***p < 0.001$, statistical difference against 50% theoretic mean (one-sample Student t test), $n = 10$ animals per group. **c** Discrimination index, obtained as the percent difference between exploration times of novel or known localization, in relation to T2 total exploration. $**p < 0.01$ when compared to CD (Student's t test), $n = 10$ mice per group. **d** Elevated Plus Maze apparatus. **e** Quantification of open arms exploration time

neurogenic capability, predominance of immature dendritic spines, and spatial memory deficits. With the aim to investigate the potential connection between microglia reactivity and neuronal dysfunction, we performed a series of in vitro experiments. Primary microglia from the cortex and hippocampus of P1-3 mice was exposed to different concentrations of palmitate (PA), the most common saturated fatty acid in western diets and present in HFD. First of all, DAPI and propidium iodide cell labeling allowed us to determine the working concentrations of PA that would not affect cultures' viability to a great extent (Fig. 6a, b). PA complexed with fatty acid-free serum albumin at 0, 125, and 500 μM was employed to study the in vitro microglial response. To this end, the levels of the pro-inflammatory cytokines TNFα and IL1β were assessed by ELISA in the conditioned media. When the microglial culture was incubated with PA at 500 μM during 24 h, while TNFα did not reach a significant increase (Fig. 6c) compared to control containing only BSA, IL1β levels were remarkably higher (Fig. 6d). In contrast, the quantities of the anti-inflammatory cytokine IL4 were significantly lower after PA exposure (Fig. 6e). Overall, these data show that PA induces a pro-inflammatory profile on primary microglial cells.

Exosomal Fraction Isolation from Palmitate-Stimulated Primary Microglial Culture and its Effect on Hippocampal Neuron Dendritic Spines

The following aim was to explore the role of exosome-like extracellular vesicles derived from PA-exposed microglia on neuronal structural plasticity. Consequently, the conditioned media from primary microglia stimulated with different PA concentrations was subjected to differential centrifugation to obtain the corresponding EV fractions. As the scheme in Fig. 7a shows, the isolation protocol included previous separation of cell debris, organelles, and apoptotic bodies at 800, 4000, and 15,000 g sequential centrifugation steps, respectively. Further ultracentrifugation at 110,000g took place to obtain the exosome-containing fraction. Labeling of this resultant fraction with uranyl acetate and examination with high-resolution transmission electron microscope allowed the verification of exosomal vesicles' morphology (Fig. 7b) and reported diameter. The analysis of the exosomal fraction showed a predominance of vesicles with a diameter around 60–70 nm (Fig. 7c). However, at least for the assayed PA concentrations (125 and 500 μM), no variations in diameter and total protein content were registered on isolated exosome-like EV fraction
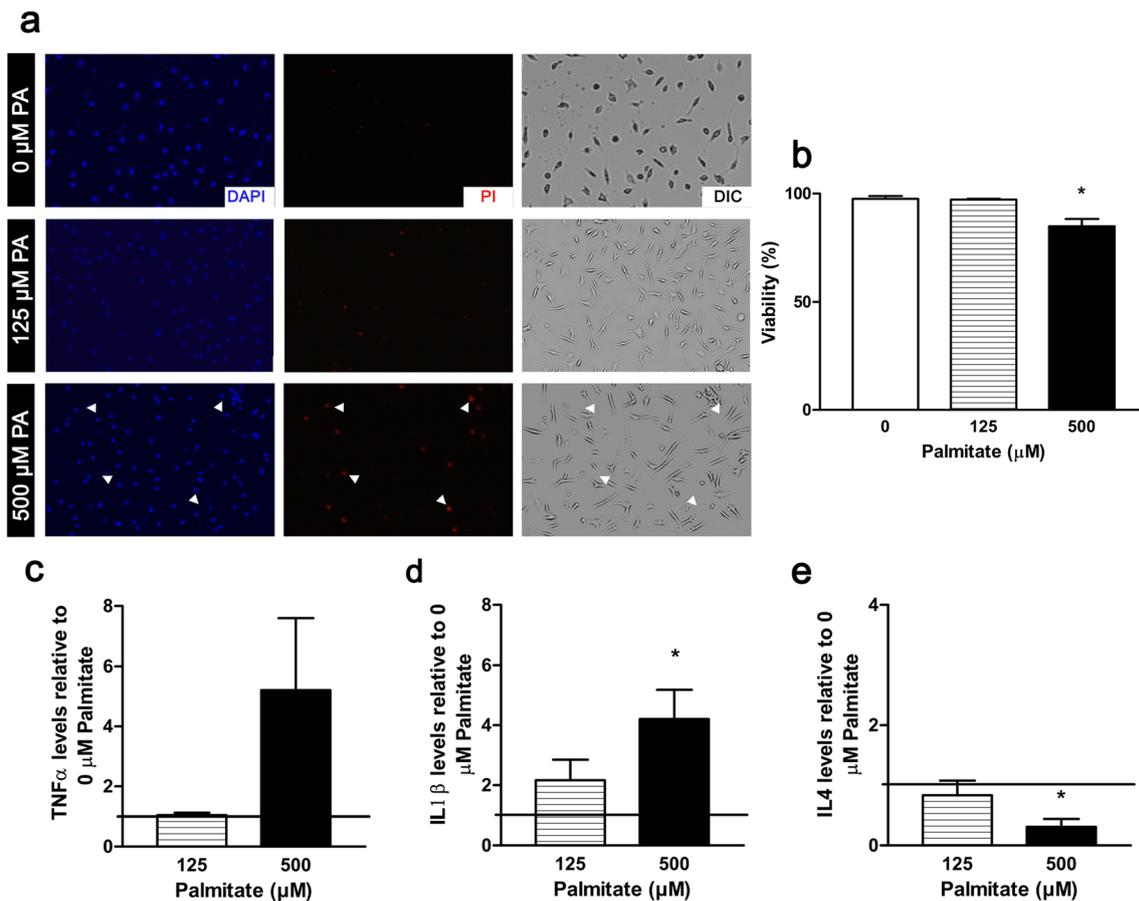
Fig. 6 Effect of the saturated fatty acid palmitate on primary microglia culture viability and secretory profile. **a** Representative images of PA-exposed microglial cells stained with DAPI and propidium iodide (PI), obtained with fluorescence microscopy. Arrowheads show dead PI positive cells and the quantification is shown in **b**. Viability is expressed as the percentage of DAPI positive nuclei negative for PI. $*p < 0.05$ when comparing 500 μM PA to control (one-way ANOVA with Tukey post hoc test). **c–e** Protein levels of cytokines in the conditioned media of microglia exposed to palmitate: TNFα (**c**), IL1β (**d**), and IL4 (**e**). Cytokine levels assessed by ELISA are normalized to control and $*p < 0.05$ represents statistical difference with 1 (0 μM PA), (one-sample Student t test)

(Fig. 7c, d). Furthermore, EVs extraction was replicated using BV2 murine microglial cell line exposed to palmitate at the same concentrations as primary microglia, with the objective of optimizing protein obtention for Western blot determinations. As it is depicted in Fig. 7e, the vesicle fraction obtained after ultracentrifugation, corresponding to exosome-like vesicles, was positive for the reported exosomal markers ALIX and TSG101.

Once we were able to characterize the exosome-like identity of the EV fraction obtained by the ultracentrifugation protocol of the conditioned media, we pursued our aim to assess the impact of exosomes derived from PA-exposed microglia in the modulation of neuronal connectivity. To that end, 14 DIV hippocampal neurons (from E18 mice) that were previously transfected with a GFP-expressing plasmid were incubated for 24 h with the exosomal vesicles released from microglia stimulated with different concentrations of PA or vehicle. Confocal z-stack reconstruction images were obtained from GFP+ dendrites of each condition (Fig. 8a) in order to analyze dendritic spine number and morphology on hippocampal dendrites. The quantification of total spine density, as well as categorization of distinct spine types according to morphology, was done following the previously mentioned procedure applied for Dil + arborizations on brain slices. First of all, as the bar graph in Fig. 8b shows, total spine density (number of spines/10 μm dendritic segment) was unaltered regardless of the experimental condition, i.e., hippocampal neurons exposed to exosomes derived from vehicle (Exo 0 μM PA) or PA-stimulated primary microglia (Exo 125–500 μM PA). Regarding spine morphology, after the exposure of hippocampal neurons to the exosomal fraction derived from primary microglia treated with PA, there was a marked effect in spine remodeling (Fig. 8c–e, significant differences for mature, mushroom, and thin spine densities, $p < 0.05$ one-way ANOVA). In particular, we found significant changes associated to incubation with exosomes derived from microglia exposed to the higher concentration of PA (500 μM PA). A significant reduction in mature spines was verified (Fig. 8c,
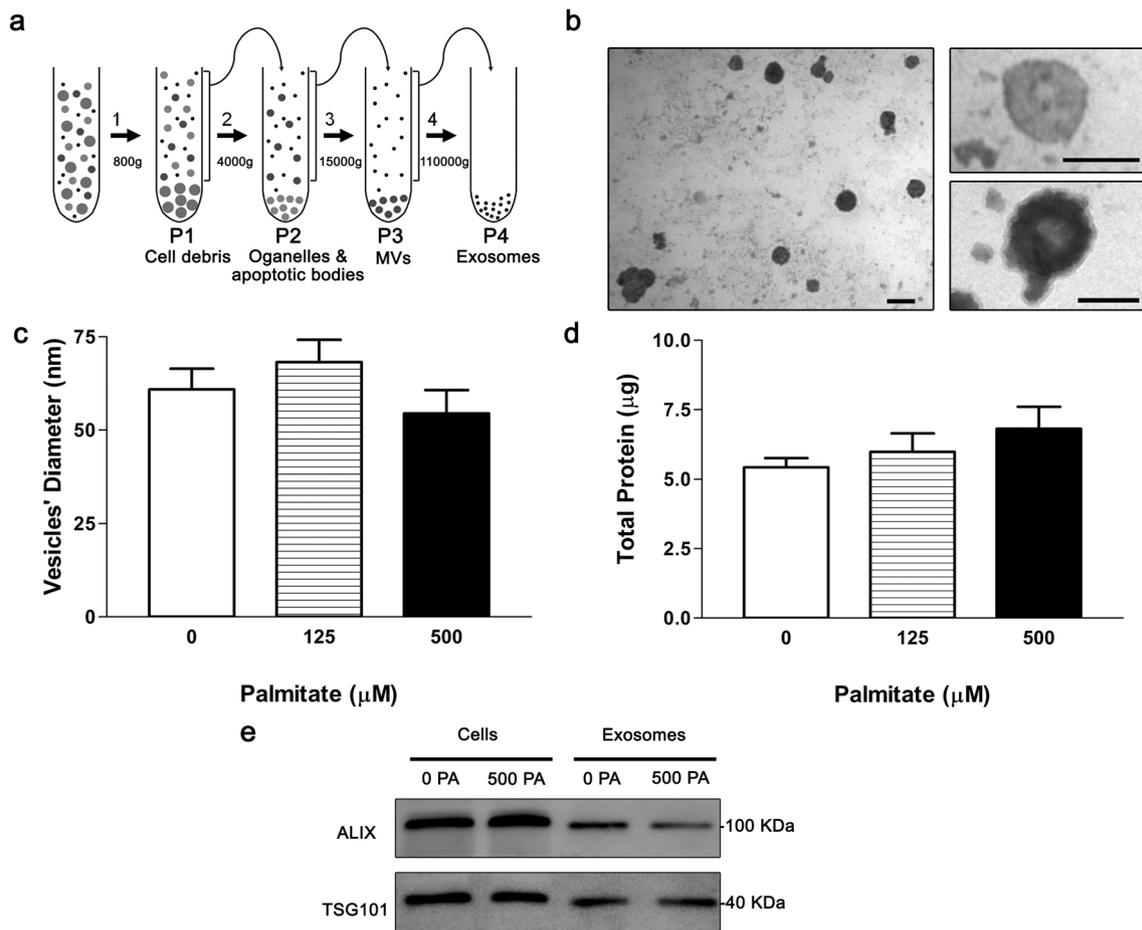
Fig. 7 Characterization of exosome-like vesicles isolated from conditioned media of microglia exposed to palmitate. **a** Exosome isolation scheme showing differential centrifugation steps. **b** Representative TEM images after exosome fraction obtained from primary microglia conditioned media, stained with uranyl acetate at different magnifications, scale bars of 100 and 50 μm. **c** Exosome-like vesicles diameter was measured in different fields of the TEM grid, from at least 16 spatially isolated vesicles. No differences in diameter were found upon PA treatment, one-way ANOVA $p > 0.05$. **d** Total micro BCA protein quantification from exosomal fraction of primary microglia exposed to control or PA containing medium, one-way ANOVA $p > 0.05$. **e** Western blot bands of exosomal markers Alix and TSG101 in control or 500 μM PA-stimulated microglial BV-2 cell line lysates and exosomal fraction obtained after ultracentrifugation at 110,000g

$p < 0.05$ Tukey post hoc contrast against Exo 0 μM PA) and, in line with this result, we found a predominance of immature thin spines (Fig. 8e, $p < 0.01$ Tukey post hoc contrast against Exo 0 μM PA). When primary microglia was stimulated with a low concentration of PA (125 μM), the corresponding exosomal fraction was associated to the same pattern of changes in spine maturity, but the differences did not reach statistical significance. As for untreated GFP+ 14 DIV neurons (Fig. 8a, upper panel), dendritic spine densities (number of spines/10 μm segment) were also calculated as a reference, 4.58 ± 0.56 total spines, 2.45 ± 0.28 mature, 2.01 ± 0.25 mushroom, and 2.83 ± 0.23 thin spines/10 μm.

Remarkably, these in vitro results regarding synaptic remodeling recapitulated the in vivo findings where structural synaptic plasticity of hippocampal CA1 neurons was studied after Dil injection to brain slices from mice consuming HFD from early stages of life (Fig. 4), thus suggesting a potential role of microglia-derived exosomes.

Discussion

The present study intended to further explore the impact of metabolic dysfunction due to an increased dietary lipid intake on hippocampal plasticity in a particularly vulnerable window of time, prior to adulthood. Our results showed that HFD had an effect on glycemia—with unaltered body weight—when administered to young mice from P21 to P60, an age parallelizing human adolescence. Pancreatic insulin content was found to be diminished, suggesting an early pancreatic dysfunction that could have later implications in the development of insulin resistance and associated disorders [57–59]. Moreover, IL1β exhibited high seric levels, with an order of
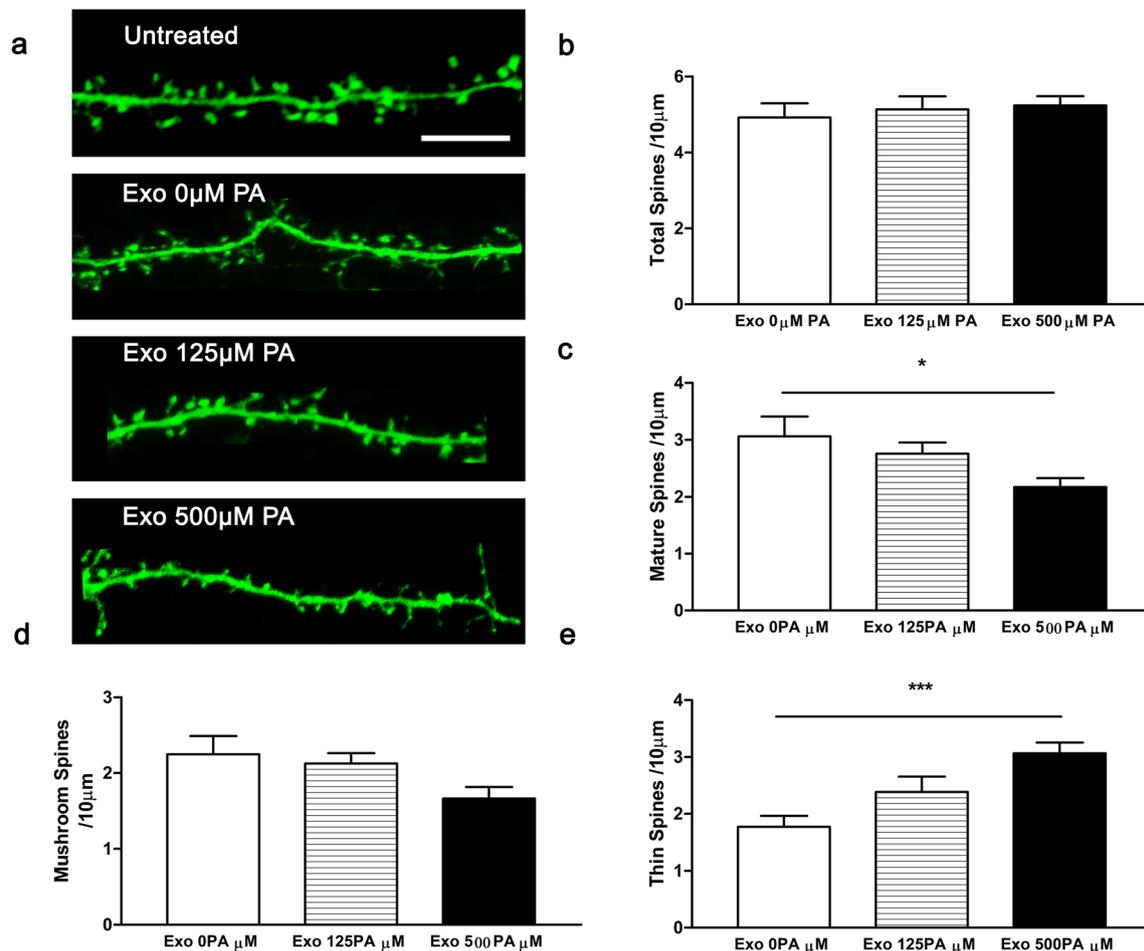
Fig. 8 Exosome-like vesicles derived from PA-stimulated primary microglia affect dendritic spine morphology in primary hippocampal neurons. **a** Representative dendritic segments of 14 DIV primary hippocampal neurons expressing transfected GFP incubated with exosome-like vesicles from primary microglia exposed to palmitate or vehicle. Images were obtained as reconstructions of z-stacks from confocal microscopy. **b–e** Number of dendritic spines normalized to 10 μm dendritic segment. Total dendritic spines (**b**), one-way-ANOVA $p > 0.05$; mature (stubby + mushroom) (**c**), one-way-ANOVA $p < 0.05$; mushroom (**d**), one-way-ANOVA $p < 0.05$ or thin (**e**) spines, one-way-ANOVA $p < 0.001$. Morphological classification was performed applying an algorithm with spine parameters: spine length and head and neck diameters, as done with CA1 dendrites in brain slice shown in Fig. 4. *$p < 0.05$ and ***$p < 0.001$ when compared to Exo 0 PA μM (Tukey post hoc test), n = dendritic segments from at least 15 neurons and two independent experiments

magnitude of increase, thus contributing to the pro-inflammatory scenario of this early and relatively short HFD exposure. In the present study, inflammation was also manifested in the hippocampus by microglial reactivity, assessed in the stratum radiatum under CA1 and the hilus of the DG, in association to a marked increase of cytokines' expression, in accordance with published results [60, 61]. The induction of a pro-inflammatory state associated to the high intake of dietary fats is probably mediated by multiple and interconnected pathways including toll-like receptors, peroxisome proliferator-activated receptors, fatty acid-binding proteins, and oxidative stress mediators reviewed in [62], highlighting the complexity of this scenario.

Several reports have linked neuroinflammation with neuronal structural plasticity impairment in different neurological disorders [63, 64]. Brain plasticity represents the intrinsic ability of CNS to react to a constantly changing environment, by functional and structural modifications. Adult neurogenesis and synaptic remodeling represent two mechanisms involved in such adaptability [65–67]. Regarding the incorporation of newborn neurons to the hippocampal circuit, in rodents, the neurogenic capability in the dentate gyrus is at its higher levels during the juvenile period with a progressive decline with aging [68]. Metabolic dysfunction in type 1 diabetes and long-term exposure to HFD is associated with a decrease in neurogenesis ability in young mice [58, 69, 70]. In line with that, in this study, we found a strong decrease in cell proliferation in the subgranular zone and less DCX+ immature granular neurons in 2-month-old HFD-fed mice. The fact that the reduction in the number of DCX+ cells occurs mainly in the A-D subpopulation, i.e. neurons with undeveloped dendritic arborization, together with the remarkably

diminished proliferation in the SGZ, suggests a weakened neurogenic process which is particularly vulnerable in its first stages as a consequence of HFD exposure. Inflammation and signaling molecules released by immune cells in the brain have been associated with impaired hippocampal neurogenesis. Microglia that expresses an inflammatory phenotype can affect cell proliferation, survival, and function of new granular neurons [71, 72]. Hence, the fact that microglia exhibits signs of reactivity in the hippocampus and especially in the hilus of the dentate gyrus, which is juxtaposed to the SGZ, emphasizes this concept.

As for the modulation of structural synaptic plasticity, events of generation, elimination, strengthening, or weakening of synapses are key targets of environmental signals. The dendritic compartment of a neuron receives input from thousands of mostly excitatory upstream neurons via synapses [73] and dendritic spines represent the *loci* where the majority of synapses occur [74]. Dendritic spines are composed of a head and a thin neck that connects them to the dendritic shaft and can have a wide variety of morphologies which appears to be critical from the functional point of view [75]. Given the fact that larger spines are able to recruit more PSD components, in particular a greater amount of AMPA receptors, the direct association of spine size and synapse strength becomes evident [76]. Larger spines, as mushroom and stubby, are considered to be mature and enable the occurrence of stronger postsynaptic currents, thus influencing neuronal activity to a greater extent [77]. Our results showed that dendritic spine morphology is affected at early stages in mice fed with HFD, with a predominance of immature spines in the CA1 subfield without changes on total spine density, suggesting potential synaptic deficits as a consequence of metabolic alterations and induced neuroinflammation. In reference to dendritic spine dynamics underlying synaptic efficacy, actin cytoskeleton and scaffold proteins involved in its remodeling are of great relevance in the fine-tuned regulation of spine morphology. Factors that regulate actin polymerization/depolymerization rates, as well as spine membrane properties, constitute key mediators of synaptic function upon different stimuli [78, 79]. In that sense, we found that levels of the scaffold protein Shank2 were notably diminished in hippocampal homogenates of HFD mice. Shank2 is part of the Shank protein family, interacting with numerous PSD components and involved in spine morphogenesis. All shank isoforms are reported to induce early maturation of spines in developing neurons and increase in spine size in mature neurons, upon overexpression [80]. Moreover, Shank2 knockdown and specific mutations in Autism Spectrum Disorders' (ASD) models as well as postmortem ASD brains are associated with synaptic dysfunction with predominance of immature thin spines [81]. The fact that we did not find significant differences in PSD-95 in HFD hippocampal homogenates by Western blot analysis might be related to the conserved spine numbers in both groups,

yet it implies the need to use more precise techniques to study changes in its distribution.

In addition to reactive microglia, low hippocampal neurogenesis and changes in dendritic spines morphology, we found a poor cognitive performance in a specific spatial hippocampal-dependent task, the novel object location recognition test. Spine numbers and morphology were reported as structural underlying events of memory formation in the rat, both in spatial and working memory hippocampal-dependent tests, such as the Morris water maze and the radial arm memory test [82]. In line with this, our results are indicative of a cognitive impairment in association with low neurogenic ability and an immature dendritic spine pattern in a neuroinflammatory context in young mice fed with HFD. Even though inflammation is one of the most important mediators of diet-induced cognitive impairment, other factors like central insulin resistance, hypothalamic-pituitary-adrenal axis activation, and diminished levels of neurotrophic factors are also relevant contributing pathways [83]. In relation to emotional processing-related behaviors, we did not find significant differences in the EPM test in 2-month-old HFD mice, similarly to what Boitard et al reported in rats exposed to juvenile HFD [84]. However, as we reported previously, a prolonged exposure to the hyperlipidic diet until 5 months of age promoted not only alterations associated to anxiety, as shown by a decreased exploration of the EPM open arms, but also concerning depressive-like behavior by increased freezing time in the tail suspension test [12], possibly suggesting differential dynamics in the implication of metabolic disorders in diverse types of behavior.

Regarding the possible mechanisms of action involved in the glial activation associated to over nutrition, free fatty acids (FFAs) are key components in high-fat diets known to contribute to lipid toxicity of many cell types [85–87]. Evidence shows that FFAs are able to cross the blood-brain barrier, and there are reports indicating an increase of their transport from circulation to the brain in contexts of metabolic disorders such as HFD exposure and metabolic syndrome [88, 89]. In fact, Spinelli et al. showed that palmitic acid is accumulated in the hippocampus of C57BL/6J mice upon HFD treatment [90]. Moreover, it has been shown that long-chain FFA can affect microglial function through the canonical toll-like receptor 4 (TLR4) that masters the inflammatory response [91, 92].

In the attempt to find possible mechanisms involved in the interplay between microglial and neuronal compartments subjected to a lipotoxic insult, the in vitro results replicated the pro-inflammatory phenotype of microglia. On the one hand, primary microglia incubated with the saturated free fatty acid palmitate presented an increase in cytokines' release, in agreement with the pro-inflammatory microenvironment found in the hippocampus of HFD mice. In this respect, experiments employing BV2 cells microglial mouse cell line also showed a pro-inflammatory profile associated to the presence of PA

[93]. On the other hand, as regards the role of microglia-neuron communication, exosomes purified from PA-stimulated primary microglia induced alterations in the morphology of dendritic spines in GFP+ hippocampal cultured neurons. Predominance of immature thin spines with an unaltered density of protrusions per dendritic segment was found in primary hippocampal neurons in the presence of exosomes purified from palmitate-stimulated microglia added to the culture medium. Therefore, microglia-neuron communication through exosomal EVs could represent a relevant phenomenon involved in neuronal dysfunction upon a metabolic insult. It is important to mention that spine analysis on GFP hippocampal neurons was also performed after incubation with the MV fraction (P3) from microglial cells exposed to palmitate and no differences were detected, neither in total number of spines nor in spine morphology (data not shown), pointing out the notion of the exosomal pathway specificity in this context.

As regards possible candidate molecules within PA microglia-derived exosomes mediating neuronal alterations, as it was previously mentioned, actin cytoskeleton regulators constitute crucial targets. For instance, molecules of diverse nature, lipids, proteins, or nucleic acids, capable of modulating the function of actin binding proteins (ABPs), such as cortactin, cofilin, and CamKIIb, are potential mediators carried in exosomal vesicles [94]. MicroRNAs represent relevant candidate molecules to study, since they are reported to be transferred within EVs from cell to cell and have a strong participation in local protein synthesis within the synaptodendritic compartment [95]. As a matter of fact, there is evidence of synaptic alterations in inflammatory contexts mediated by miRNAs such as miR-146a-5p, loaded in microglial EVs [96]. Also, it was recently reported that scaffold protein Shank2, which we found diminished in HFD hippocampi, is a direct target of miR-137. miR-137 downregulates protein translation of several proteins at the postsynaptic locus such as AMPA receptors and Shank2 and, interestingly, both events, overexpression of miR-137 and downregulation of Shank2, are associated to neurodevelopmental and neuropsychiatric disorders [97].

Further experiments must be conducted for in-depth study of the ideas that have arisen from our work suggesting that exosomes from microglia stimulated by components of high-fat diets may contribute to alter dendritic spine morphology of pyramidal neurons in the hippocampus of young mice. Importantly, EV-mediated microglia-neuron communication might be acting among a set of microglia-derived signals such as glutamate, ROS, cytokines, and chemokines [98], establishing complex response patterns. What is more, direct effects to neurons and mechanisms involving indirect effects mediated by other interactions, with astrocytes for instance, cannot be excluded.

Neurobehavioral, morphological, neurochemical, and pharmacological evidence suggest that brain circuits are in active remodeling and maturation during adolescence [2, 99]. In that sense, our study indicates that during the peri-adolescent period, the brain could be especially susceptible to environmental factors as high-fat diet promoting chronic inflammation and inducing relevant changes in neuronal connectivity associated to cognitive alterations, effects that could have a long-lasting impact on the adult brain. Our study contributes to understand the complexity of the relationship between glia and neurons in the hippocampus under an inflammatory scenario promoted by a high-fat diet, during this relevant life period when neuroendocrine systems' flexibility in ongoing maturation can be severely affected.

Compliance with Ethical Standards

All animal experiments followed the NIH Guide for the Care and Use of Laboratory Animals and were approved by the Ethical Committee of the Institute of Biology and Experimental Medicine.

Conflict of Interest The authors declare that they have no competing interests.

References

1. Patton GC, Olsson CA, Skirbekk V, Saffery R, Wlodek ME, Azzopardi PS, Stonawski M, Rasmussen B et al (2018) Adolescence and the next generation. Nature 554(7693):458–466. http://sci-hub.tw/10.1038/nature25759

2. Casey BJ, Duhoux S, Malter Cohen M (2010) Adolescence: what do transmission, transition, and translation have to do with it? Neuron 67(5):749–760. http://sci-hub.tw/10.1016/j.neuron.2010.08.033

3. Walker DM, Bell MR, Flores C, Gulley JM, Willing J, Paul MJ (2017) Adolescence and reward: making sense of neural and behavioral changes amid the chaos. J Neurosci 37(45):10855–10866. http://sci-hub.tw/10.1523/JNEUROSCI.1834-17.2017

4. Spear LP (2000) The adolescent brain and age-related behavioral manifestations. Neurosci Biobehav Rev 24(4):417–463

5. Shin SY, Han SH, Woo RS, Jang SH, Min SS (2016) Adolescent mice show anxiety- and aggressive-like behavior and the reduction

of long-term potentiation in mossy fiber-CA3 synapses after neo-natal maternal separation. Neuroscience 316:221–231. http://sci-hub.tw/10.1016/j.neuroscience.2015.12.041

6. Spear LP (2013) Adolescent neurodevelopment. J Adolesc Health 52(2 Suppl 2):S7–S13. http://sci-hub.tw/10.1016/j.jadohealth.2012.05.006

7. Venn AJ, Thomson RJ, Schmidt MD, Cleland VJ, Curry BA, Gennat HC, Dwyer T (2007) Overweight and obesity from childhood to adulthood: a follow-up of participants in the 1985 Australian Schools Health and Fitness Survey. Med J Aust 186(9):458–460

8. Dey A, Hao S, Wosiski-Kuhn M, Stranahan AM (2017) Glucocorticoid-mediated activation of GSK3beta promotes tau phosphorylation and impairs memory in type 2 diabetes. Neurobiol Aging 57:75–83. http://sci-hub.tw/10.1016/j.neurobiolaging.2017.05.010

9. Xu WL, Atti AR, Gatz M, Pedersen NL, Johansson B, Fratiglioni L (2011) Midlife overweight and obesity increase late-life dementia risk: a population-based twin study. Neurology 76(18):1568–1574

10. McNay EC, Ong CT, McCrimmon RJ, Cresswell J, Bogan JS, Sherwin RS (2010) Hippocampal memory processes are modulated by insulin and high-fat-induced insulin resistance. Neurobiol Learn Mem 93(4):546–553. http://sci-hub.tw/10.1016/j.nlm.2010.02.002

11. Whitmer RA, Gustafson DR, Barrett-Connor E, Haan MN, Gunderson EP, Yaffe K (2008) Central obesity and increased risk of dementia more than three decades later. Neurology 71(14):1057–1064. http://sci-hub.tw/10.1212/01.wnl.0000306313.89165.ef

12. Vinuesa A, Pomilio C, Menafra M, Bonaventura MM, Garay L, Mercogliano MF, Schillaci R, Lux Lantos V et al (2016) Juvenile exposure to a high fat diet promotes behavioral and limbic alterations in the absence of obesity. Psychoneuroendocrinology 72:22–33. http://sci-hub.tw/10.1016/j.psyneuen.2016.06.004

13. Paolicelli RC, Bolasco G, Pagani F, Maggi L, Scianni M, Panzanelli P, Giustetto M, Ferreira TA et al (2011) Synaptic pruning by microglia is necessary for normal brain development. Science 333(6048):1456–1458. http://sci-hub.tw/10.1126/science.1202529

14. Kramer-Albers EM, Hill AF (2016) Extracellular vesicles: interneural shuttles of complex messages. Curr Opin Neurobiol 39:101–107. http://sci-hub.tw/10.1016/j.conb.2016.04.016

15. Budnik V, Ruiz-Canada C, Wendler F (2016) Extracellular vesicles round off communication in the nervous system. Nat Rev Neurosci 17(3):160–172. http://sci-hub.tw/10.1038/nrn.2015.29

16. Rajendran L, Bali J, Barr MM, Court FA, Kramer-Albers EM, Picou F, Raposo G, van der Vos KE et al (2014) Emerging roles of extracellular vesicles in the nervous system. J Neurosci 34(46):15482–15489. http://sci-hub.tw/10.1523/JNEUROSCI.3258-14.2014

17. Lai CP, Breakefield XO (2012) Role of exosomes/microvesicles in the nervous system and use in emerging therapies. Front Physiol 3:228. http://sci-hub.tw/10.3389/fphys.2012.00228

18. Colombo M, Raposo G, Thery C (2014) Biogenesis, secretion, and intercellular interactions of exosomes and other extracellular vesicles. Annu Rev Cell Dev Biol 30:255–289. http://sci-hub.tw/10.1146/annurev-cellbio-101512-122326

19. Thery C, Ostrowski M, Segura E (2009) Membrane vesicles as conveyors of immune responses. Nat Rev Immunol 9(8):581–593. http://sci-hub.tw/10.1038/nri2567

20. Cocucci E, Racchetti G, Meldolesi J (2009) Shedding microvesicles: artefacts no more. Trends Cell Biol 19(2):43–51. http://sci-hub.tw/10.1016/j.tcb.2008.11.003

21. Trajkovic K, Hsu C, Chiantia S, Rajendran L, Wenzel D, Wieland F, Schwille P, Brugger B et al (2008) Ceramide triggers budding of exosome vesicles into multivesicular endosomes. Science 319(5867):1244–1247. http://sci-hub.tw/10.1126/science.1153124

22. Stuffers S, Sem Wegner C, Stenmark H, Brech A (2009) Multivesicular endosome biogenesis in the absence of ESCRTs.

Traffic 10(7):925–937. http://sci-hub.tw/10.1111/j.1600-0854.2009.00920.x

23. van Niel G, D'Angelo G, Raposo G (2018) Shedding light on the cell biology of extracellular vesicles. Nat Rev Mol Cell Biol. http://sci-hub.tw/10.1038/nrm.2017.125

24. Potolicchio I, Carven GJ, Xu X, Stipp C, Riese RJ, Stern LJ, Santambrogio L (2005) Proteomic analysis of microglia-derived exosomes: metabolic role of the aminopeptidase CD13 in neuropeptide catabolism. J Immunol 175(4):2237–2243

25. Abels ER, Breakefield XO (2016) Introduction to extracellular vesicles: biogenesis, RNA cargo selection, content, release, and uptake. Cell Mol Neurobiol 36(3):301–312. http://sci-hub.tw/10.1007/s10571-016-0366-z

26. Bernimoulin M, Waters EK, Foy M, Steele BM, Sullivan M, Falet H, Walsh MT, Barteneva N et al (2009) Differential stimulation of monocytic cells results in distinct populations of microparticles. J Thromb Haemost 7(6):1019–1028. http://sci-hub.tw/10.1111/j.1538-7836.2009.03434.x

27. Turola E, Furlan R, Bianco F, Matteoli M, Verderio C (2012) Microglial microvesicle secretion and intercellular signaling. Front Physiol 3:149. http://sci-hub.tw/10.3389/fphys.2012.00149

28. Bahrini I, Song JH, Diez D, Hanayama R (2015) Neuronal exosomes facilitate synaptic pruning by up-regulating complement factors in microglia. Sci Rep 5:7989. http://sci-hub.tw/10.1038/srep07989

29. Fruhbeis C, Frohlich D, Kuo WP, Kramer-Albers EM (2013) Extracellular vesicles as mediators of neuron-glia communication. Front Cell Neurosci 7:182. http://sci-hub.tw/10.3389/fncel.2013.00182

30. Joshi P, Benussi L, Furlan R, Ghidoni R, Verderio C (2015) Extracellular vesicles in Alzheimer's disease: friends or foes? Focus on abeta-vesicle interaction. Int J Mol Sci 16(3):4800–4813. http://sci-hub.tw/10.3390/ijms16034800

31. Kong SM, Chan BK, Park JS, Hill KJ, Aitken JB, Cottle L, Farghaian H, Cole AR et al (2014) Parkinson's disease-linked human PARK9/ATP13A2 maintains zinc homeostasis and promotes alpha-Synuclein externalization via exosomes. Hum Mol Genet 23(11):2816–2833. http://sci-hub.tw/10.1093/hmg/ddu099

32. Paolicelli RC, Bergamini G, Rajendran L (2018) Cell-to-cell communication by extracellular vesicles: focus on microglia. Neuroscience. http://sci-hub.tw/10.1016/j.neuroscience.2018.04.003

33. Yang Y, Boza-Serrano A, Dunning CJR, Clausen BH, Lambertsen KL, Deierborg T (2018) Inflammation leads to distinct populations of extracellular vesicles from microglia. J Neuroinflammation 15(1):168. http://sci-hub.tw/10.1186/s12974-018-1204-7

34. Verderio C, Muzio L, Turola E, Bergami A, Novellino L, Ruffini F, Riganti L, Corradini I et al (2012) Myeloid microvesicles are a marker and therapeutic target for neuroinflammation. Ann Neurol 72(4):610–624. http://sci-hub.tw/10.1002/ana.23627

35. Bianco F, Pravettoni E, Colombo A, Schenk U, Moller T, Matteoli M, Verderio C (2005) Astrocyte-derived ATP induces vesicle shedding and IL-1 beta release from microglia. J Immunol 174(11):7268–7277

36. Takenouchi T, Tsukimoto M, Iwamaru Y, Sugama S, Sekiyama K, Sato M, Kojima S, Hashimoto M et al (2015) Extracellular ATP induces unconventional release of glyceraldehyde-3-phosphate dehydrogenase from microglial cells. Immunol Lett 167(2):116–124. http://sci-hub.tw/10.1016/j.imlet.2015.08.002

37. Huang S, Ge X, Yu J, Han Z, Yin Z, Li Y, Chen F, Wang H et al (2018) Increased miR-124-3p in microglial exosomes following traumatic brain injury inhibits neuronal inflammation and contributes to neurite outgrowth via their transfer into neurons. FASEB J 32(1):512–528. http://sci-hub.tw/10.1096/fj.201700673R

38. Dutta S, Sengupta P (2016) Men and mice: relating their ages. Life Sci 152:244–248. http://sci-hub.tw/10.1016/j.lfs.2015.10.025

39. Valdivia S, Patrone A, Reynaldo M, Perello M (2014) Acute high fat diet consumption activates the mesolimbic circuit and requires orexin signaling in a mouse model. PLoSOne 9(1):e87478

40. Bonaventura MM, Catalano PN, Chamson-Reig A, Arany E, Hill D, Bettler B, Saravia F, Libertun C et al (2008) GABAB receptors and glucose homeostasis: evaluation in GABAB receptor knockout mice. Am J Physiol Endocrinol Metab 294(1):E157–E167

41. Beauquis J, Vinuesa A, Pomilio C, Pavia P, Galvan V, Saravia F (2014) Neuronal and glial alterations, increased anxiety, and cognitive impairment before hippocampal amyloid deposition in PDAPP mice, model of Alzheimer's disease. Hippocampus 24(3):257–269

42. Beauquis J, Homo-Delarche F, Giroix MH, Ehses J, Coulaud J, Roig P, Portha B, De Nicola AF et al (2010) Hippocampal neurovascular and hypothalamic-pituitary-adrenal axis alterations in spontaneously type 2 diabetic GK rats. Exp Neurol 222(1): 125–134

43. Pomilio C, Pavia P, Gorojod RM, Vinuesa A, Alaimo A, Galvan V, Kotler ML, Beauquis J et al (2016) Glial alterations from early to late stages in a model of Alzheimer's disease: evidence of autophagy involvement in Abeta internalization. Hippocampus 26(2): 194–210. http://sci-hub.tw/10.1002/hipo.22503

44. Pozzo-Miller LD, Inoue T, Murphy DD (1999) Estradiol increases spine density and NMDA-dependent Ca2+ transients in spines of CA1 pyramidal neurons from hippocampal slices. J Neurophysiol 81(3):1404–1411. http://sci-hub.tw/10.1152/jn.1999.81.3.1404

45. Giachero M, Calfa GD, Molina VA (2013) Hippocampal structural plasticity accompanies the resulting contextual fear memory following stress and fear conditioning. Learn Mem 20(11):611–616. http://sci-hub.tw/10.1101/lm.031724.113

46. Koh IY, Lindquist WB, Zito K, Nimchinsky EA, Svoboda K (2002) An image analysis algorithm for dendritic spines. Neural Comput 14(6):1283–1310. http://sci-hub.tw/10.1162/089976602753712945

47. Tyler WJ, Pozzo-Miller L (2003) Miniature synaptic transmission and BDNF modulate dendritic spine growth and form in rat CA1 neurones. J Physiol 553(Pt 2):497–509. http://sci-hub.tw/10.1113/jphysiol.2003.052639

48. Calfa G, Chapleau CA, Campbell S, Inoue T, Morse SJ, Lubin FD, Pozzo-Miller L (2012) HDAC activity is required for BDNF to increase quantal neurotransmitter release and dendritic spine density in CA1 pyramidal neurons. Hippocampus 22(7):1493–1500. http://sci-hub.tw/10.1002/hipo.20990

49. Bradford MM (1976) A rapid and sensitive method for the quantitation of microgram quantities of protein utilizing the principle of protein-dye binding. Anal Biochem 7(72):248–254

50. Pfaffl MW (2001) A new mathematical model for relative quantification in real-time RT-PCR. Nucleic Acids Res 29(9):e45

51. Filipello F, Morini R, Corradini I, Zerbi V, Canzi A, Michalski B, Erreni M, Markicevic M et al (2018) The microglial innate immune receptor TREM2 is required for synapse elimination and normal brain connectivity. Immunity 48(5):979–991 e978. http://sci-hub.tw/10.1016/j.immuni.2018.04.016

52. Oliveira AF, Cunha DA, Ladriere L, Igoillo-Esteve M, Bugliani M, Marchetti P, Cnop M (2015) In vitro use of free fatty acids bound to albumin: a comparison of protocols. BioTechniques 58(5):228–233. http://sci-hub.tw/10.2144/000114285

53. Shelke GV, Lasser C, Gho YS, Lotvall J (2014) Importance of exosome depletion protocols to eliminate functional and RNA-containing extracellular vesicles from fetal bovine serum. J Extracell Vesicles 3. http://sci-hub.tw/10.3402/jev.v3.24783

54. Kuhn HG, Dickinson-Anson H, Gage FH (1996) Neurogenesis in the dentate gyrus of the adult rat: age-related decrease of neuronal progenitor proliferation. J Neurosci 16(6):2027–2033

55. Chapleau CA, Larimore JL, Theibert A, Pozzo-Miller L (2009) Modulation of dendritic spine development and plasticity by BDNF and vesicular trafficking: fundamental roles in

56. On V, Zahedi A, Ethell IM, Bhanu B (2017) Automated spatio-temporal analysis of dendritic spines and related protein dynamics. PLoS One 12(8):e0182958. http://sci-hub.tw/10.1371/journal.pone.0182958

57. Guillausseau PJ, Meas T, Virally M, Laloi-Michelin M, Medeau V, Kevorkian JP (2008) Abnormalities in insulin secretion in type 2 diabetes mellitus. Diabetes Metab 34(Suppl 2):S43–S48. http://sci-hub.tw/10.1016/S1262-3636(08)73394-9

58. Boitard C, Etchamendy N, Sauvant J, Aubert A, Tronel S, Marighetto A, Laye S, Ferreira G (2012) Juvenile, but not adult exposure to high-fat diet impairs relational memory and hippocampal neurogenesis in mice. Hippocampus 22(11):2095–2100

59. Lee H, Lee S, Cho IH, Lee SJ (2013) Toll-like receptors: sensor molecules for detecting damage to the nervous system. Curr Protein Pept Sci 14(1):33–42

60. Sobesky JL, Barrientos RM, De May HS, Thompson BM, Weber MD, Watkins LR, Maier SF (2014) High-fat diet consumption disrupts memory and primes elevations in hippocampal IL-1beta, an effect that can be prevented with dietary reversal or IL-1 receptor antagonism. Brain Behav Immun 42:22–32

61. Guillemot-Legris O, Muccioli GG (2017) Obesity-induced neuro-inflammation: beyond the hypothalamus. Trends Neurosci 40(4): 237–253. http://sci-hub.tw/10.1016/j.tins.2017.02.005

62. Johnson AR, Milner JJ, Makowski L (2012) The inflammation highway: metabolism accelerates inflammatory traffic in obesity. Immunol Rev 249(1):218–238. http://sci-hub.tw/10.1111/j.1600-065X.2012.01151.x

63. Sobue A, Ito N, Nagai T, Shan W, Hada K, Nakajima A, Murakami Y, Mouri A et al (2018) Astroglial major histocompatibility complex class I following immune activation leads to behavioral and neuropathological changes. Glia 66(5):1034–1052. http://sci-hub.tw/10.1002/glia.23299

64. Zou C, Shi Y, Ohli J, Schuller U, Dorostkar MM, Herms J (2016) Neuroinflammation impairs adaptive structural plasticity of dendritic spines in a preclinical model of Alzheimer's disease. Acta Neuropathol 131(2):235–246. http://sci-hub.tw/10.1007/s00401-015-1527-8

65. Kelly KM, Nadon NL, Morrison JH, Thibault O, Barnes CA, Blalock EM (2006) The neurobiology of aging. Epilepsy Res 68(Suppl 1):S5–S20. http://sci-hub.tw/10.1016/j.eplepsyres.2005.07.015

66. Pascual-Leone A, Freitas C, Oberman L, Horvath JC, Halko M, Eldaief M, Bashir S, Vernet M et al (2011) Characterizing brain cortical plasticity and network dynamics across the age-span in health and disease with TMS-EEG and TMS-fMRI. Brain Topogr 24(3–4):302–315. http://sci-hub.tw/10.1007/s10548-011-0196-8

67. Rosenzweig ES, Barnes CA (2003) Impact of aging on hippocampal function: plasticity, network dynamics, and cognition. Prog Neurobiol 69(3):143–179

68. Saravia F, Beauquis J, Pietranera L, De Nicola A (2007) Neuroprotective effects of estradiol in hippocampal neurons and glia of middle age mice. Psychoneuroendocrinology 32:480–492

69. Boitard C, Cavaroc A, Sauvant J, Aubert A, Castanon N, Laye S, Ferreira G (2014) Impairment of hippocampal-dependent memory induced by juvenile high-fat diet intake is associated with enhanced hippocampal inflammation in rats. Brain Behav Immun 40:9–17

70. Valladolid-Acebes I, Fole A, Martin M, Morales L, Cano MV, Ruiz-Gayo M, Del Olmo N (2013) Spatial memory impairment and changes in hippocampal morphology are triggered by high-fat diets in adolescent mice. Is there a role of leptin? Neurobiol Learn Mem 106:18–25

71. Kohman RA, Rhodes JS (2013) Neurogenesis, inflammation and behavior. Brain Behav Immun 27(1):22–32. http://sci-hub.tw/10.1016/j.bbi.2012.09.003

neurodevelopmental disorders associated with mental retardation and autism. J Neurodev Disord 1(3):185–196

72. Belarbi K, Rosi S (2013) Modulation of adult-born neurons in the inflamed hippocampus. Front Cell Neurosci 7:145. http://sci-hub.tw/10.3389/fncel.2013.00145

73. Adrian M, Kusters R, Wierenga CJ, Storm C, Hoogenraad CC, Kapitein LC (2014) Barriers in the brain: resolving dendritic spine morphology and compartmentalization. Front Neuroanat 8:142. http://sci-hub.tw/10.3389/fnana.2014.00142

74. Yuste R, Bonhoeffer T (2001) Morphological changes in dendritic spines associated with long-term synaptic plasticity. Annu Rev Neurosci 24:1071–1089. http://sci-hub.tw/10.1146/annurev.neuro.24.1.1071

75. Luengo-Sanchez S, Fernaud-Espinosa I, Bielza C, Benavides-Piccione R, Larranaga P, DeFelipe J (2018) 3D morphology-based clustering and simulation of human pyramidal cell dendritic spines. PLoS Comput Biol 14(6):e1006221. http://sci-hub.tw/10.1371/journal.pcbi.1006221

76. Honkura N, Matsuzaki M, Noguchi J, Ellis-Davies GC, Kasai H (2008) The subspine organization of actin fibers regulates the structure and plasticity of dendritic spines. Neuron 57(5):719–729. http://sci-hub.tw/10.1016/j.neuron.2008.01.013

77. McKinney RA (2010) Excitatory amino acid involvement in dendritic spine formation, maintenance and remodelling. J Physiol 588(Pt 1):107–116. http://sci-hub.tw/10.1113/jphysiol.2009.178905

78. Holtmaat A, Svoboda K (2009) Experience-dependent structural synaptic plasticity in the mammalian brain. Nat Rev Neurosci 10(9):647–658. http://sci-hub.tw/10.1038/nrn2699

79. Kasai H, Fukuda M, Watanabe S, Hayashi-Takagi A, Noguchi J (2010) Structural dynamics of dendritic spines in memory and cognition. Trends Neurosci 33(3):121–129. http://sci-hub.tw/10.1016/j.tins.2010.01.001

80. Sarowar T, Grabrucker AM (2016) Actin-dependent alterations of dendritic spine morphology in shankopathies. Neural Plast 2016:8051861. http://sci-hub.tw/10.1155/2016/8051861

81. Berkel S, Tang W, Trevino M, Vogt M, Obenhaus HA, Gass P, Scherer SW, Sprengel R et al (2012) Inherited and de novo SHANK2 variants associated with autism spectrum disorder impair neuronal morphogenesis and physiology. Hum Mol Genet 21(2):344–357. http://sci-hub.tw/10.1093/hmg/ddr470

82. Mahmmoud RR, Sase S, Aher YD, Sase A, Groger M, Mokhtar M, Hoger H, Lubec G (2015) Spatial and working memory is linked to spine density and mushroom spines. PLoS One 10(10):e0139739. http://sci-hub.tw/10.1371/journal.pone.0139739

83. Freeman LR, Haley-Zitlin V, Rosenberger DS, Granholm AC (2014) Damaging effects of a high-fat diet to the brain and cognition: a review of proposed mechanisms. Nutr Neurosci 17(6):241–251

84. Boitard C, Maroun M, Tantot F, Cavaroc A, Sauvant J, Marchand A, Laye S, Capuron L et al (2015) Juvenile obesity enhances emotional memory and amygdala plasticity through glucocorticoids. J Neurosci 35(9):4092–4103

85. Li S, Li H, Yang D, Yu X, Irwin DM, Niu G, Tan H (2017) Excessive autophagy activation and increased apoptosis are associated with palmitic acid-induced cardiomyocyte insulin resistance. J Diabetes Res 2017:2376893. http://sci-hub.tw/10.1155/2017/2376893

86. Mayer CM, Belsham DD (2010) Palmitate attenuates insulin signaling and induces endoplasmic reticulum stress and apoptosis in hypothalamic neurons: rescue of resistance and apoptosis through adenosine 5′ monophosphate-activated protein kinase activation. Endocrinology 151(2):576–585. http://sci-hub.tw/10.1210/en.2009-1122

87. Tang S, Wu W, Tang W, Ge Z, Wang H, Hong T, Zhu D, Bi Y (2017) Suppression of Rho-kinase 1 is responsible for insulin regulation of the AMPK/SREBP-1c pathway in skeletal muscle cells exposed to palmitate. Acta Diabetol 54(7):635–644. http://sci-hub.tw/10.1007/s00592-017-0976-z

88. Gupta N, Goel K, Shah P, Misra A (2012) Childhood obesity in developing countries: epidemiology, determinants, and prevention. Endocr Rev 33(1):48–70

89. Karmi A, Iozzo P, Viljanen A, Hirvonen J, Fielding BA, Virtanen K, Oikonen V, Kemppainen J et al (2010) Increased brain fatty acid uptake in metabolic syndrome. Diabetes 59(9):2171–2177. http://sci-hub.tw/10.2337/db09-0138

90. Spinelli M, Fusco S, Mainardi M, Scala F, Natale F, Lapenta R, Mattera A, Rinaudo M et al (2017) Brain insulin resistance impairs hippocampal synaptic plasticity and memory by increasing GluA1 palmitoylation through FoxO3a. Nat Commun 8(1):2009. http://sci-hub.tw/10.1038/s41467-017-02221-9

91. Wang Z, Liu D, Wang F, Liu S, Zhao S, Ling EA, Hao A (2012) Saturated fatty acids activate microglia via Toll-like receptor 4/NF-kappaB signalling. Br J Nutr 107(2):229–241. http://sci-hub.tw/10.1017/S0007114511002868

92. Chunchai T, Chattipakorn N, Chattipakorn SC (2017) The possible factors affecting microglial activation in cases of obesity with cognitive dysfunction. Metab Brain Dis. http://sci-hub.tw/10.1007/s11011-017-0151-9

93. Tracy LM, Bergqvist F, Ivanova EV, Jacobsen KT, Iverfeldt K (2013) Exposure to the saturated free fatty acid palmitate alters BV-2 microglia inflammatory response. J Mol Neurosci 51(3):805–812. http://sci-hub.tw/10.1007/s12031-013-0068-7

94. Bellot A, Guivernau B, Tajes M, Bosch-Morato M, Valls-Comamala V, Munoz FJ (2014) The structure and function of actin cytoskeleton in mature glutamatergic dendritic spines. Brain Res 1573:1–16. http://sci-hub.tw/10.1016/j.brainres.2014.05.024

95. Schratt G (2009) microRNAs at the synapse. Nat Rev Neurosci 10(12):842–849. http://sci-hub.tw/10.1038/nrn2763

96. Prada I, Gabrielli M, Turola E, Iorio A, D'Arrigo G, Parolisi R, De Luca M, Pacifici M et al (2018) Glia-to-neuron transfer of miRNAs via extracellular vesicles: a new mechanism underlying inflammation-induced synaptic alterations. Acta Neuropathol 135(4):529–550. http://sci-hub.tw/10.1007/s00401-017-1803-x

97. de Sena Cortabitarte A, Berkel S, Cristian FB, Fischer C, Rappold GA (2018) A direct regulatory link between microRNA-137 and SHANK2: implications for neuropsychiatric disorders. J Neurodev Disord 10(1):15. http://sci-hub.tw/10.1186/s11689-018-9233-1

98. Takeuchi H, Jin S, Wang J, Zhang G, Kawanokuchi J, Kuno R, Sonobe Y, Mizuno T et al (2006) Tumor necrosis factor-alpha induces neurotoxicity via glutamate release from hemichannels of activated microglia in an autocrine manner. J Biol Chem 281(30):21362–21368. http://sci-hub.tw/10.1074/jbc.M600504200

99. Giedd JN, Blumenthal J, Jeffries NO, Castellanos FX, Liu H, Zijdenbos A, Paus T, Evans AC et al (1999) Brain development during childhood and adolescence: a longitudinal MRI study. Nat Neurosci 2(10):861–863. http://sci-hub.tw/10.1038/13158